Gondwana Research 86 (2020) 250–265

Contents lists available at ScienceDirect

Gondwana Research

journal homepage: www.elsevier.com/locate/gr

Genesis of the supergiant Huayangchuan carbonatite-hosted uranium-polymetallic deposit in the Qinling Orogen, Central China

Hui Zheng [a,b], Huayong Chen [a,c,*], Chao Wu [a,*], Hongjun Jiang [d], Cheng Gao [d], Qingqing Kang [d], Chunsi Yang [a,b], Dequan Wang [d], Chun-kit Lai [e]

[a] Key Laboratory of Mineralogy and Metallogeny, Guangzhou Institute of Geochemistry, Chinese Academy of Sciences, Guangzhou 510640, China
[b] University of Chinese Academy of Sciences, Beijing 100049, China
[c] Guangdong Provincial Key Laboratory of Mineral Physics and Materials, Guangzhou 510640, China
[d] Team 224 of Sino Shaanxi Nuclear Industry Group, Xi'an 710100, China
[e] Faculty of Science, Universiti Brunei Darussalam, Gadong BE1410, Brunei Darussalam

ARTICLE INFO

Article history:
Received 5 August 2019
Received in revised form 17 May 2020
Accepted 20 May 2020
Available online 3 July 2020

Handling Editor: F. Pirajno

Keywords:
Huayangchuan carbonatite-hosted U-Nb-REE-Ba-Sr deposit
Paragenesis
Multistage mineralization
Ore-forming process
Qinling Orogen

ABSTRACT

The newly-discovered supergiant Huayangchuan uranium (U)-polymetallic deposit is situated in the Qinling Orogen, Central China. The deposit contains economic endowments of U, Nb, Pb, Se, Sr, Ba and REEs, some of which (e.g., U, Se, and Sr) reaching super-large scale. Pyrochlore, allanite, monazite, barite-celestite and galena are the major ore minerals at Huayangchuan. Uranium is mainly hosted in the primary mineral of pyrochlore, and the mineralization is mainly hosted in or associated with carbonatite dikes.

According to the mineral assemblages and crosscutting relationships, the alteration/mineralization at Huayangchuan comprises four stages, i.e., pegmatite REE mineralization (I), main mineralization (II), skarn mineralization (III) and post-ore alteration (IV). Coarse-grained euhedral allanite is the main Stage I REE mineral, and the pegmatite-hosted REE mineralization (ca. 1.8 Ga) occurs mostly in the shallow-level of northwestern Huayangchuan, corresponding to the Paleoproterozoic Xiong'er Group volcanic rocks (1.80–1.75 Ga) in the southern margin of North China Block. Carbonatite-hosted Stage II mineralization contributes to the majority of U-Nb-REE-Ba-Sr resources, and is controlled by the Huayangchuan Fault. Stage II mineralization can be further divided into the sulfate mineralization (barite-celestite) (II-A), alkali-rich U mineralization (aegirine-augite + pyrochlore + uraninite + uranothorite) (II-B) and REE (allanite + monazite + chevkinite)-U (pyrochlore + uraninite) mineralization (II-C) substages. Stage II mineralization may have occurred during the Late Triassic Mianlue Ocean closure. Skarn mineralization contributed to the majority of Pb and minor U-REE (uraninite-allanite) resources at Huayangchuan, and is spatially associated with the Late Cretaceous-Early Jurassic (Yanshanian) Huashan and Laoniushan granites. We suggested that hydrothermal fluids derived from the Laoniushan and Huashan granites may have reacted with the Triassic carbonatites, and formed the Huayangchuan Pb skarn mineralization.

The mantle-derived Triassic carbonatites may have been fertilized by the U-rich subducting oceanic sediments, and were further enriched through reacting with the Proterozoic U-REE-rich pegmatite wallrocks at Huayangchuan. Ore-forming elements were likely transported in metal complexes (F^-, PO_4^{3-}, CO_3^{2-} and SO_4^{2-}), and deposited with the dilution of the complex concentration. This may have formed the distinct vertical mineralization zoning, i.e., sodic fenite-related alkali-U mineralization at depths and potassic fenite-related REE-U mineralization at shallow level.

1. Introduction

Proterozoic unconformity-controlled and granite-related deposits represent the world's most important type of uranium (U) deposits. In contrast, carbonatite-hosted U deposits are rare, with the only few examples reported including the Phalaborwa and Sankopsdrif deposits (South Africa), and the Manitou Islands deposit (Canada) (Dahlkamp, 1993; NEA/IAEA, 2016; Woolley and Kempe, 1989; Woolley and Kjarsgaard, 2008). For the large Phalaborwa deposit, its low U grade (average 0.004%) and resource tonnage (several thousand tonnes) indicate that uranium is only a byproduct (Groves and Vielreicher, 2001).

The Qinling Orogen in Central China is a well-endowed mineral province for Au, Mo, Ag, Pb, Zn, Ba, Hg and Sb (Chen et al., 2009; Chen,

* Corresponding authors.
E-mail address: huayongchen@gig.ac.cn (H. Chen).

https://doi.org/10.1016/j.gr.2020.05.016
1342-937X/

2010; Li et al., 2007). The carbonatite-hosted Huayangchuan deposit is located on the northern margin of North China Block. Despite being first discovered back in 1956 by the Jinduicheng Geological Team, discovery of major orebodies was only made since 2012 by #224 team of the Sino Shaanxi Nuclear Industry Group. Uranium resource at Huayangchuan was considered to be supergiant scale (>20 kt (large scale); Dahlkamp, 2009), and will likely supersede the Xiangshan deposit (Jiangxi Province) to become the largest uranium deposit in China. In addition, the Huayangchuan deposit contains economic endowments of Se, Sr, Nb, REE, Ba, Pb, Ag and Bi. Previous studies focused predominately on the petrological and geochemical characteristics of the carbonatites in/around Huayangchuan (He et al., 2016; Hui et al., 2017; Hui and He, 2016; Reguir et al., 2012; Song et al., 2016; Wang et al., 2011; Xu et al., 2007; Yu, 1992), and concluded that the carbonatites have an igneous origin. However, some aspects about the U-Nb-REE mineralization are still unclear, notably any metallogenic link with the local pegmatite and carbonatite dikes, the geochemistry/paragenesis of the complex mineral assemblages and any zoning pattern, and the mechanism of uranium ore precipitation. Based on systematic drill-core logging, mineralization mapping and petrographic observation in this study, we established a detailed alteration/mineralization paragenetic sequence, and presented new data on the major ore mineral compositions and preliminary mineral distribution patterns. We discussed the ore-forming process of this unusual type of carbonatite-related U-dominated deposit, and its association with the tectonic events in the Qinling Orogen.

2. Geological setting

The Huayangchuan U-polymetallic deposit is situated in Shaanxi Province and geologically in the Qinling Orogen (Fig. 1a). The orogen contains four tectonic units, i.e., (from north to south) southern margin

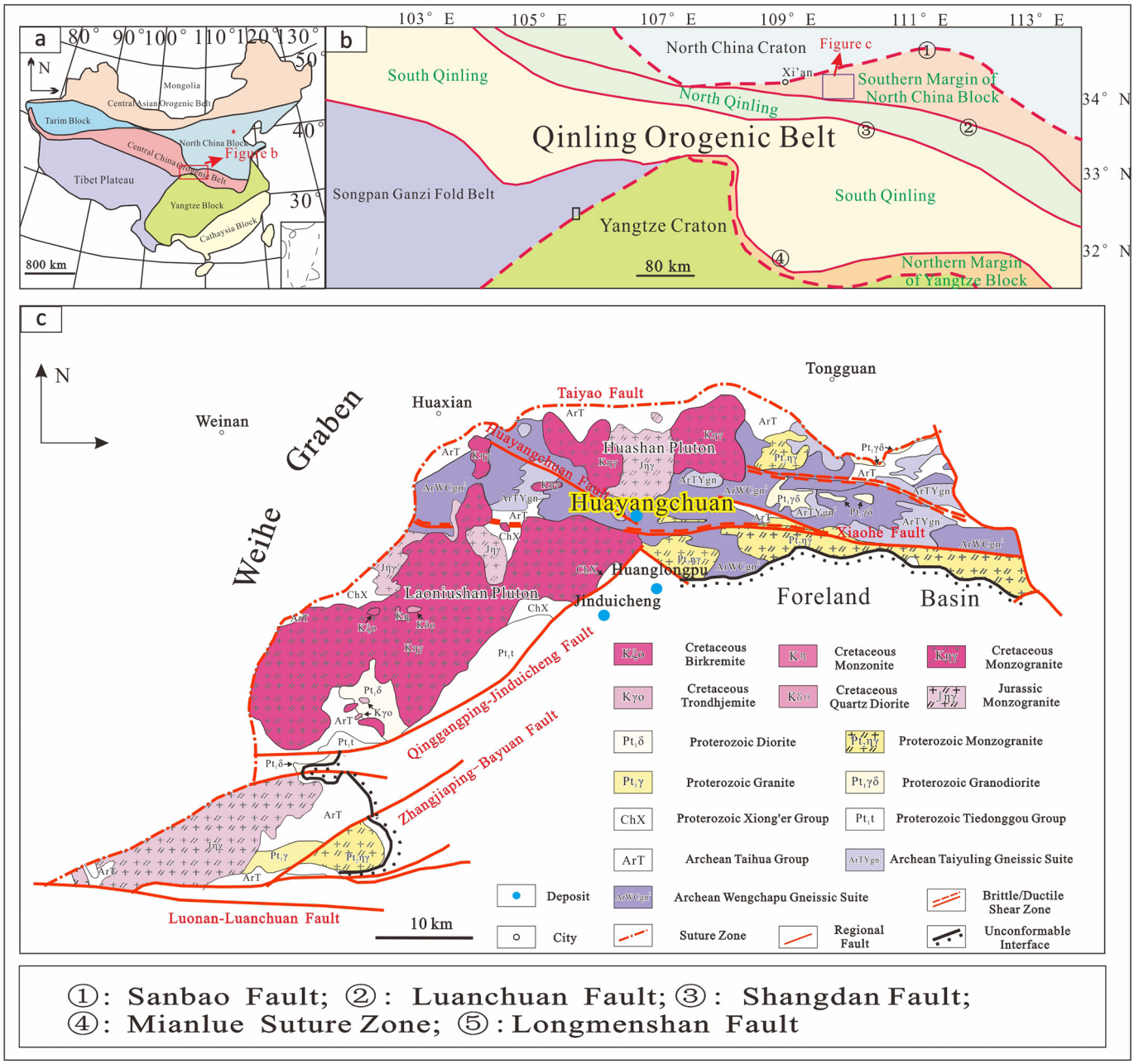

Fig. 1. (a) Geological sketch map of China. (b) Regional tectonic map of Qinling Orogenic Belt (modified from Chen, 2010). (c) Geological map of the Huayangchuan district (modified from Gao et al., 2017).

of North China Block, North Qinling, South Qinling and northern margin of Yangtze Block. These tectonic units are separated by the Luanchuan, Shangdan and Mianlue faults, respectively (Fig. 1b). Apart from the Huayangchuan deposit, the Jinduicheng porphyry Mo deposit (0.98 Mt @ 0.099%) and Huanglongpu carbonatite-related Mo(-Re) deposit are also discovered in the district (Fig. 1c; Li et al., 2007).

Three major stratigraphic units in the district are namely the Archean Taihua Group (Gp.), the Proterozoic Tiedonggou and Xiong'er Groups. The Taihua Group comprises a high-grade metamorphic suite, including the biotite-(amphibole)-plagioclase migmatite and biotite-albite gneiss. The Tiedonggou Group comprises meta-clastic rocks such as quartzite and (mica)-quartz schist. The Xiong'er Group comprises a rift-type volcanic-sedimentary suite, including bimodal volcanics and their associated terrestrial volcaniclastic rocks.

The Huayangchuan district has experienced multiphase deformation and metamorphism, resulting in a complex crustal architecture including many metamorphic core complexes, folds and faults. Major faults (e.g., Taiyao, Xiaohe, Huayangchuan; Fig. 1c) in the district are WNW- to EW-trending, and are crosscut by NE-trending secondary structures.

Intrusive rocks are widespread in the district, including the Archean gneissic TTG (tonalite-trondhjemite-granodiorite) suite (i.e., the Taiyuling and Wengchapu gneiss), Proterozoic granitoids (mainly dioritic to granitic), Jurassic monzogranite and Cretaceous granitoids (mainly quartz diorite, monzonite and monzogranite) (Fig. 1c).

3. Deposit geology

Exposed stratigraphy at Huayangchuan comprises mainly the Taihua Gp. biotite-plagioclase gneiss, which is generally NNW-trending and moderately dipping (~60°). The NW-trending and ore-controlling Huayangchuan fault is 500–1000 m long and crosscut by NE-trending structures (Fig. 2). Multiphase magmatism at Huayangchuan is represented by the Archean Wengchapu TTG gneiss, Proterozoic monzogranite, granite porphyry and pegmatite dikes, Triassic carbonatite dikes, and Jurassic-Cretaceous granitoids. The Proterozoic monzogranite in eastern Huayangchuan comprises K-feldspar (30–40 vol%), plagioclase (30–35 vol%), quartz (20–25 vol%) and biotite (3–8 vol%). The Proterozoic granite porphyry and pegmatite dykes at Huayangchuan are distributed along the NW-trending structural lineament. Granite porphyry is composed of K-feldspar (50–60 vol%), plagioclase (10–15 vol%), quartz (15–20 vol%), biotite (3–5 vol%) and amphibole (1–3 vol%), microcline is the major phenocryst. The Proterozoic pegmatite is mainly composed of coarse-grained K-feldspar (60–70 vol%), quartz (30–35 vol%) with minor biotite, and accessory minerals including allanite, apatite and zircon. The Triassic carbonatite dykes (0.01–1 m thick) are the main ore host at Huayangchuan, and are generally NW-trending and NE-dipping. These carbonatite dykes commonly crosscut the early Archean gneiss, TTG suite, and the Proterozoic granite porphyry and pegmatite. The Jurassic and Cretaceous granitoids are exposed in northern and southern Huayangchuan (i.e., Huashan and Laoniushan plutons) (Fig. 2), and mainly consist of fine-grained monzogranite and medium-grained monzonite, respectively.

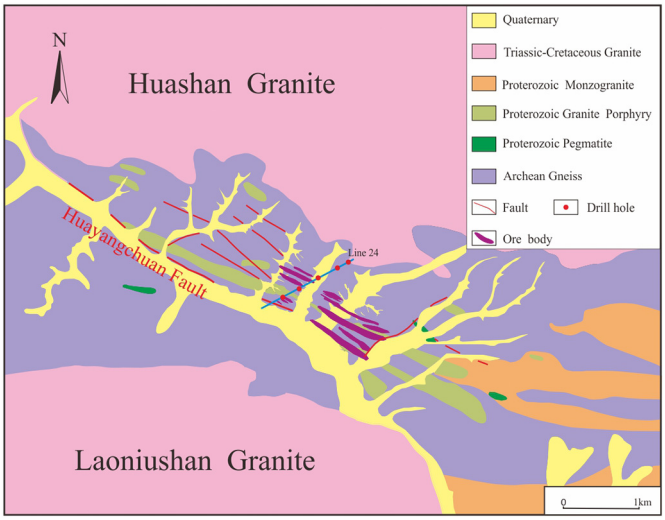

Fig. 2. Simplified geologic map of the Huayangchuan deposit.

Mineralization at Huayangchuan commonly occurs as veinlets and (locally) stockworks in the carbonatite dykes. Over 40 ore and gangue minerals were identified at Huayangchuan. Ore minerals include mainly pyrochlore, allanite, monazite, barite-celestite and galena, and minor uraninite, uranothorite and chevkinite. Major gangue minerals include calcite, aegirine-augite, titanite, apatite, phlogopite, garnet, amphibole and biotite. Major mineral assemblages include (1) monazite + allanite + pyrochlore + phlogopite + calcite, (2) pyrochlore + apatite + titanite + calcite + aegirine-augite, and (3) garnet + biotite + amphibole + magnetite + pyrite + galena. Ore-related alteration styles at Huayangchuan include mainly fenitization and potassic alteration.

4. Sampling and EPMA analysis

In this study, over 2000 core samples were collected from 19 drill-holes at Huayangchuan. 450 polished thin sections were prepared and observed under the microscope to reveal the alteration/mineralization paragenetic relationships. Mineral compositions were determined with electron probe microanalysis (EPMA) (Table 1 and Supplementary Data), using a JXA-JEOL-8230 at the School of Earth Science and Technology, Southwest Petroleum University. The analytical conditions include: 15 kV accelerating voltage, 20 nA beam current with 1–10 μm beam diameter. The following materials were used for calibration: TiO_2 (Ti), $MgCaSi_2O_6$ (Ca, Mg, Si), $NaAlSi_3O_8$ (Na, Al), $KAlSi_3O_8$ (K), $CaMnSi_2O_6$ (Mn), $FeCr_2O_4$ (Fe), $Ca_5(PO_4)_3F$ (P), CeF_3 (Ce), NdF_3 (Nd), LaF_3 (La, F), $SrSO_4$ (Sr), $BaSO_4$ (Ba, S), Nb metal (Nb), Y metal (Y), Ta metal (Ta), UO_2 (U), ThO_2 (Th), and $PbCrO_4$ (Pb).

5. Alteration and mineralization paragenesis

Based on mineral assemblages and crosscutting relationships, four mineralization stages at Huayangchuan were identified (Fig. 3), i.e., (I) pegmatite REE mineralization, (II) main U-Nb-REE-Ba-Sr mineralization, (III) skarn mineralization and (IV) post-mineralization. Stage II can be further divided into three substages, i.e., sulfate Ba-Sr (barite-celestite) mineralization (II-A), alkali-rich U (aegirine-augite + pyrochlore + uraninite + uranothorite) mineralization (II-B) and REE (monazite + allanite + chevkinite) + U (pyrochlore + uraninite) mineralization (II-C).

Stage I: Pegmatite REE mineralization

At Huayangchuan, massive pegmatite and dykes were found both in outcrops (Figs. 2 and 4a) and at depth (Fig. 4b), commonly crosscutting the Taihua Gp. wallrocks. The Huayangchuan pegmatite contains coarse-grained microcline and quartz, which intergrew with disseminated allanite and show local graphic texture (Fig. 4b–d). Allanite is the main REE ore mineral in the pegmatite, and is rich in some LREE oxides (Ce_2O_3: 7.26–8.08 wt%; La_2O_3: 3.53–4.09 wt%; Nd_2O_3: 1.90–1.95 wt %) and ThO_2 (2.39–3.25 wt%). Locally, the allanite can be up to centimeters in size, and is easily identified (as black/dark-grey elongated grains) in hand-specimens and under the microscope (Fig. 4e–g). Most Stage I allanite grains contain a reddish radiation-damaged rim (Fig. 4h), i.e., uraninite formed by allanite decomposition. Furthermore, some allanite grains coexist with coarse-grained zircon and apatite (Fig. 4i).

Table 1
The representative electron microprobe analyses of pyrochlore in the Huayangchuan deposit. (bd: below the detect line; /: undetected element).

	Pyrochlore1(coexisting with monazite)								
Comment	zk-2403-32-4	zk-2403-32-3	zk-2403-32-5	zk-2403-31-1	zk-2403-31-2	zk-2403-31-5	zk-2403-31-6	zk-2403-31-7	zk-2403-31-8
MgO	bd	bd	0.01	0.02	0.04	bd	bd	bd	bd
Al_2O_3	bd	0.02	bd	bd	bd	bd	bd	bd	bd
SiO_2	0.04	0.15	0.34	0.67	0.72	2.32	1.47	0.97	0.20
MnO	0.11	0.15	0.27	0.50	0.48	0.12	0.11	0.10	0.15
FeO	0.58	0.55	0.74	1.42	1.26	1.61	2.14	1.40	1.24
CaO	13.29	13.07	13.24	9.55	7.32	7.89	9.42	10.64	6.02
TiO_2	14.63	13.91	14.89	15.95	16.28	15.91	17.07	14.90	18.07
Nb_2O_5	34.98	35.72	35.09	36.28	34.14	35.89	34.13	37.09	34.82
Ta_2O_5	/	/	/	/	/	bd	bd	bd	bd
ThO_2	bd	0.05	0.04	bd	bd	bd	bd	bd	bd
UO_2	29.19	29.17	29.09	29.70	30.46	28.62	30.63	29.05	31.59
Ce_2O_3	0.33	0.39	0.45	0.66	0.67	0.65	0.79	0.65	0.55
PbO	0.42	0.47	0.48	0.71	0.27	0.37	0.38	0.43	0.45
F	/	/	/	/	/	0.07	0.23	0.50	0.14
Y_2O_3	0.04	0.06	0.04	0.03	bd	0.07	0.14	0.08	0.09
Total	93.73	93.91	94.95	95.86	92.48	93.49	96.41	95.61	93.27
a.p.f.u. on the basis of B = 2 (B including Mg, Si, Ti, Nb and Ta, Atencio et al., 2010)									
Mg	bd	bd	0.00	0.00	0.00	bd	bd	bd	bd
Al	bd	0.00	bd	bd	bd	bd	bd	bd	bd
Si	0.00	0.01	0.03	0.05	0.05	0.15	0.10	0.07	0.01
Mn	0.01	0.01	0.02	0.03	0.03	0.01	0.01	0.01	0.01
Fe	0.04	0.03	0.05	0.08	0.08	0.09	0.12	0.08	0.07
Ca	1.06	1.05	1.05	0.72	0.57	0.55	0.68	0.79	0.44
Ti	0.82	0.79	0.83	0.85	0.89	0.78	0.86	0.77	0.92
Nb	1.18	1.21	1.17	1.15	1.11	1.06	1.04	1.16	1.07
Ta	/	/	/	/	/	bd	bd	bd	bd
Th	bd	0.00	0.00	bd	bd	bd	bd	bd	bd
U	0.48	0.49	0.48	0.47	0.49	0.42	0.46	0.45	0.48
Ce	0.01	0.01	0.01	0.02	0.02	0.02	0.02	0.02	0.01
Pb	0.01	0.01	0.01	0.01	0.00	0.01	0.01	0.01	0.01
F	/	/	/	/	/	0.01	0.05	0.11	0.03
Y	0.00	0.00	0.00	0.00	bd	0.00	0.00	0.00	0.00

	Pyrochlore2 (coexisting with apatite)								
Comment	zk-1607-5-6	zk-1607-5-7	zk-1607-5-8	zk-1607-1	zk-1607-27-1	zk-1607-27-2	zk-1607-27-3	zk-1607-36-1	zk-1607-36-2
MgO	bd	bd	bd	bd	bd	0.02	bd	bd	0.01
Al_2O_3	bd	bd	bd	bd	bd	0.07	bd	0.02	0.02
SiO_2	0.03	bd	bd	bd	0.09	2.50	0.10	bd	bd
MnO	0.22	0.24	0.20	0.12	0.04	0.80	0.23	0.91	0.28
FeO	0.34	0.33	0.18	0.28	0.44	0.43	0.21	0.14	bd
CaO	13.79	14.94	15.45	14.33	14.89	10.26	14.07	15.38	14.60
TiO_2	17.99	17.56	16.90	16.31	18.53	17.72	17.13	16.64	19.21
Nb_2O_5	31.46	30.88	32.78	32.01	29.55	29.07	31.79	33.15	28.89
Ta_2O_5	/	/	/	/	/	/	/	/	/
ThO_2	0.17	0.12	bd	0.14	0.13	0.04	0.08	0.02	0.07
UO_2	32.12	31.72	31.85	31.42	31.86	30.93	31.49	31.11	31.04
Ce_2O_3	0.09	0.03	bd	bd	0.16	0.00	0.10	0.05	0.37
PbO	0.60	0.55	0.36	0.48	0.48	0.55	0.58	0.40	0.46
F	/	/	/	/	/	/	/	/	/
a.p.f.u. on the basis of B = 2 (B including Mg, Si, Ti, Nb and Ta, Atencio et al., 2010)									
Y_2O_3	0.17	0.17	0.10	0.20	0.19	0.10	0.15	0.10	0.22
Total	97.04	96.56	97.82	95.96	96.68	93.06	96.29	98.08	95.50
Mg	bd	bd	bd	bd	bd	0.00	bd	bd	0.00
Al	bd	bd	bd	bd	bd	0.01	bd	0.00	0.00
Si	0.00	bd	bd	bd	0.01	0.19	0.01	bd	bd
Mn	0.01	0.02	0.01	0.01	0.00	0.05	0.01	0.06	0.02
Fe	0.02	0.02	0.01	0.02	0.03	0.03	0.01	0.01	bd
Ca	1.06	1.18	1.20	1.15	1.17	0.83	1.11	1.20	1.14
Ti	0.98	0.97	0.92	0.92	1.02	1.00	0.95	0.91	1.05
Nb	1.02	1.03	1.08	1.08	0.98	0.99	1.05	1.09	0.95
Ta	/	/	/	/	/	/	/	/	/
Th	0.00	0.00	bd	0.00	0.00	0.00	0.00	0.00	0.00
U	0.51	0.52	0.51	0.52	0.52	0.52	0.51	0.50	0.50
Ce	0.00	0.00	bd	bd	0.00	0.00	0.00	0.00	0.01
Pb	0.01	0.01	0.01	0.01	0.01	0.01	0.01	0.01	0.01
F	/	/	/	/	/	/	/	/	/
Y	0.01	0.01	0.00	0.01	0.01	0.00	0.01	0.00	0.01

Pyrochlore1(coexisting with monazite)					Pyrochlore2 (coexisting with apatite)				
zk-5604-62-1	zk-5604-62-2	zk-5604-62-3	zk-5604-62-4	zk-5604-62-5	zk-1607-5-1	zk-1607-5-2	zk-1607-5-3	zk-1607-5-4	zk-1607-5-5
bd	bd	0.03	bd	bd	bd	0.03	bd	0.02	bd
bd	0.03	bd	0.02	bd	bd	bd	bd	bd	bd
bd	0.02	bd	bd	0.02	bd	2.40	0.01	1.72	0.77
bd	bd	0.03	bd	0.02	0.24	0.55	0.35	0.45	0.38
0.65	1.20	0.46	0.32	0.71	0.51	1.30	0.26	0.36	0.34
16.55	17.91	17.21	17.11	16.95	13.33	8.89	13.78	5.47	9.05
14.02	11.97	19.29	19.92	17.65	15.16	18.63	18.04	19.27	18.74
40.10	42.24	30.53	30.08	33.81	32.80	30.11	30.01	32.43	31.32
0.10	bd	bd	bd	bd	/	/	/	/	/
0.06	bd	bd	0.04	bd	bd	0.04	0.05	0.03	0.18
27.13	25.18	30.97	31.71	29.87	31.17	31.90	31.88	33.56	32.82
bd	bd	0.03	0.01	0.11	0.05	bd	bd	0.05	0.08
0.40	0.42	0.42	0.44	0.46	0.50	0.43	0.50	0.56	0.51
0.28	0.45	0.24	0.47	0.23	/	/	/	/	/
0.08	0.04	0.04	0.06	0.05	0.11	0.06	0.12	0.13	0.14
99.25	99.27	99.15	100.00	99.82	93.89	94.39	95.06	94.03	94.40
a.p.f.u. on the basis of B = 2 (B including Mg, Si, Ti, Nb and Ta, Atencio et al., 2010)									
bd	bd	0.00	bd	bd	bd	0.00	bd	0.00	bd
bd	0.00	bd	0.00	bd	bd	bd	bd	bd	bd
bd	0.00	bd	bd	0.00	bd	0.17	0.00	0.12	0.05
bd	bd	0.00	bd	0.00	0.02	0.03	0.02	0.03	0.02
0.04	0.07	0.03	0.02	0.04	0.03	0.08	0.02	0.02	0.02
1.24	1.36	1.30	1.28	1.27	1.09	0.69	1.09	0.40	0.69
0.73	0.64	1.02	1.05	0.93	0.87	1.01	1.00	0.99	1.00
1.26	1.36	0.97	0.95	1.07	1.13	0.99	1.00	1.01	1.00
0.00	bd	bd	bd	bd	/	/	/	/	/
0.00	bd	bd	0.00	bd	bd	0.00	0.00	0.00	0.00
0.42	0.40	0.49	0.49	0.46	0.53	0.51	0.52	0.51	0.52
bd	bd	0.00	0.00	0.00	0.00	bd	bd	0.00	0.00
0.01	0.01	0.01	0.01	0.01	0.01	0.01	0.01	0.01	0.01
0.06	0.10	0.05	0.10	0.05	/	/	/	/	/
0.00	0.00	0.00	0.00	0.00	0.00	0.00	0.00	0.00	0.01

Pyrochlore2 (coexisting with apatite)					Pyrochlore3 (coexisting with titanite)				
zk-1607-36-4	zk-1607-36-3	zk-1607-27-1	zk-1607-27-2	zk-1607-27-3	zk-1003-13-2	zk-1003-2-1	zk-1003-2-2	zk-2404-17-1	zk-2404-17-2
bd	bd	bd	bd	0.02	bd	bd	0.02	bd	0.01
bd	bd	0.03	0.08	0.03	0.04	0.03	0.06	bd	bd
0.24	0.13	bd	bd	bd	0.05	bd	2.51	3.29	bd
0.14	0.22	0.05	0.08	0.09	0.09	0.24	0.39	0.51	0.28
0.42	0.29	1.14	1.10	0.90	0.88	1.33	1.25	1.75	0.34
12.50	15.13	15.83	15.77	15.42	14.37	14.59	8.89	7.29	15.36
16.18	16.44	16.09	14.69	16.06	12.93	12.13	14.54	17.29	15.02
34.17	33.26	34.86	37.36	34.55	37.98	38.37	36.53	33.85	34.42
/	/	bd	bd	bd	/	/	/	/	/
0.10	0.08	0.11	0.09	0.07	0.06	0.02	0.04	0.07	0.11
30.10	30.58	27.63	26.28	27.03	28.04	27.88	29.65	31.85	31.26
0.25	0.07	1.30	1.61	2.06	0.03	bd	0.04	bd	bd
0.76	0.48	0.49	0.56	0.62	0.36	0.77	0.58	0.48	0.42
/	/	0.46	0.33	0.16	/	/	/	/	/
a.p.f.u. on the basis of B = 2 (B including Mg, Si, Ti, Nb and Ta, Atencio et al., 2010)									
0.10	0.13	0.08	0.07	0.05	0.09	0.06	0.09	0.04	0.09
95.08	97.02	97.88	97.87	96.99	94.93	96.00	94.58	96.51	97.32
bd	bd	bd	bd	0.00	bd	bd	0.00	bd	0.00
bd	bd	0.00	0.01	0.00	0.00	0.00	0.01	bd	bd
0.02	0.01	bd	bd	bd	0.00	bd	0.18	0.23	bd
0.01	0.01	0.00	0.01	0.01	0.01	0.02	0.02	0.03	0.02
0.03	0.02	0.07	0.07	0.05	0.05	0.08	0.08	0.10	0.02
0.97	1.18	1.22	1.21	1.19	1.14	1.18	0.69	0.55	1.23
0.88	0.90	0.87	0.79	0.87	0.72	0.69	0.79	0.92	0.84
1.12	1.10	1.13	1.21	1.13	1.27	1.31	1.20	1.08	1.16
/	/	bd	bd	bd	/	/	/	/	/
0.00	0.00	0.00	0.00	0.00	0.00	0.00	0.00	0.00	0.00
0.49	0.50	0.44	0.42	0.43	0.46	0.47	0.48	0.50	0.52
0.01	0.00	0.03	0.04	0.05	0.00	bd	0.00	bd	bd
0.01	0.01	0.01	0.01	0.01	0.01	0.01	0.01	0.01	0.01
/	/	0.10	0.07	0.04	/	/	/	/	/
0.00	0.00	0.00	0.00	0.00	0.00	0.00	0.00	0.00	0.00

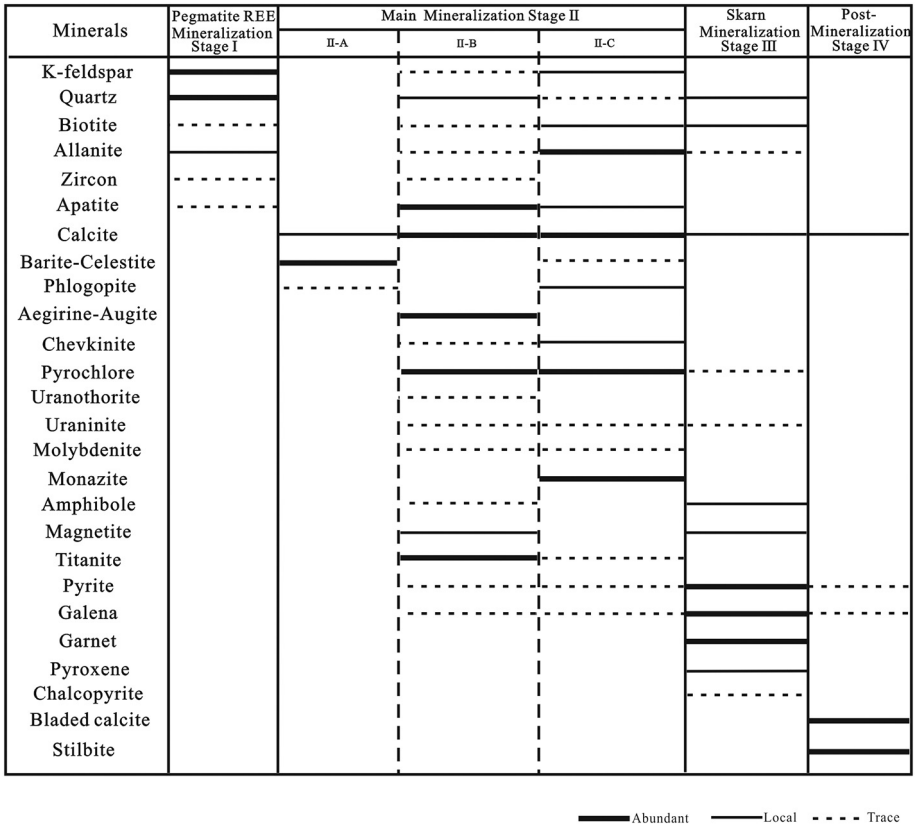

Fig. 3. Mineral paragenesis of the Huayangchuan deposit.

Stage II: Main U-Nb-REE-Ba-Sr mineralization

This stage is closely associated with carbonatite, with calcite being the main mineral. The carbonatite occurs generally as dikes or veins cutting the Archean wallrocks and Stage I pegmatite. Mineralized carbonatite veins are commonly millimeter- to several centimeter-thick. As above-mentioned, this stage can be further divided into the sulfate (Sr-Ba) mineralization (II-A), alkali-rich U mineralization (II-B) and REE-U mineralization (II-C) substages. Mineralization occurs partly in the carbonatite dikes (all Stage II-A and minor Stage II-B), and partly along the contact between the carbonatites and wallrocks/pegmatite.

o (1) Stage II-A: Sulfate (Sr-Ba) mineralization

The Sr-Ba resource of this substage is hosted mainly in the celestite-barite transition series (pure celestite and barite are rare). This substage comprises the calcite + celestite-barite + phlogopite assemblage. For most REE carbonatite deposits, sulfate minerals are very common. Xie et al. (2009) suggested that the initial ore-fluids of the Maoniuping carbonatite REE deposit were SO_4-rich, as indicated by melt-fluid inclusions. Recent experimental and thermodynamic modelling studies show that sulfate complexes are highly effective in transporting REEs, even more effective than chloride complexes (Cui et al., 2019). Similarly, the Huayangchuan carbonatite also contains abundant REE resource, and the sulfate substage also occurred before the other main-ore substages. Sulfates dominated by barite are light-yellow in hand-specimens (Fig. 5a), whilst the celestite-dominated ones are euhedral coarse-grained and cerulean in colour (Fig. 5b). Yellowish-green celestite-barite-series disseminated minerals or aggregates (Fig. 5c–d) commonly intergrew with calcite and phlogopite (Fig. 5e–f). EPMA analysis of Stage II-A sulfates (Supplementary Data) indicates a clear barite-celestite transition instead of pure barite (70% BaO) and celestite (60% SrO).

o (2) Stage II-B: Alkali-rich U mineralization

This substage is characterized by abundant pyrochlore (UO_2: 26.28–33.56 wt%; Nb_2O_5: 28.89–38.37 wt%; TiO_2: 12.13–19.27 wt%; CaO: 5.47–15.83 wt%; PbO: 0.36–0.77 wt%; Table 1), which belongs to betafite (Fig. 6). Based on the classification of pyrochlore group minerals (Hogarth, 1977; Atencio et al., 2010), Substage II-B pyrochlore data plot mainly in the betafite field, and no microlite is identified due to the absence of Ta (Fig. 6). The pyrochlore coexists with minor uraninite and uranothorite, together with calcite, aegirine-augite, amphibole, apatite, titanite, magnetite, biotite, allanite, quartz, magnetite and sulfides (mainly pyrite and galena). Aegirine-augite is the main alkaline (Na-rich) mineral at Huayangchuan, which mainly occurs in two mineral assemblages, i.e., with or without U-Nb mineralization. The ore-barren aegirine-augite is usually dark-green, coarse-grained (up to several centimeters) euhedral, and intergrown with calcite (Fig. 7a–b). In contrast, the aegirine-augite associated with pyrochlore, calcite and minor sulfides is commonly fine-medium-grained subhedral. The two Stage II-B mineral assemblages are (1) aegirine-augite + calcite + pyrochlore + apatite (+ uraninite + sulfides) (Fig. 7c), and (2) aegirine-augite + calcite + pyrochlore + titanite (+ sulfides) (Fig. 7d). In assemblage (1), pyrochlore is red, euhedral and medium-coarse grained (0.2–3 mm), usually with idiomorphic texture and growth zoning (Fig. 7e). Apatite is fine-grained and euhedral, and occurs as fluorapatite aggregates. Uraninite commonly occurs in/around the pyrochlore core (Fig. 7f). In assemblage (2), pyrochlore is fine-medium grained (<0.5 mm) subhedral, and coexists with titanite, aegirine-augite, calcite, galena, magnetite and quartz (Fig. 7d and g). Titanite is usually brown, medium-coarse-grained euhedral-subhedral with local idiomorphic texture (Fig. 7d). The fine-grained magnetite and quartz mainly occur with aegirine-augite (Fig. 7e and g). However, another assemblage, i.e., ore-barren aegirine-augite coexisting with calcite, with minor

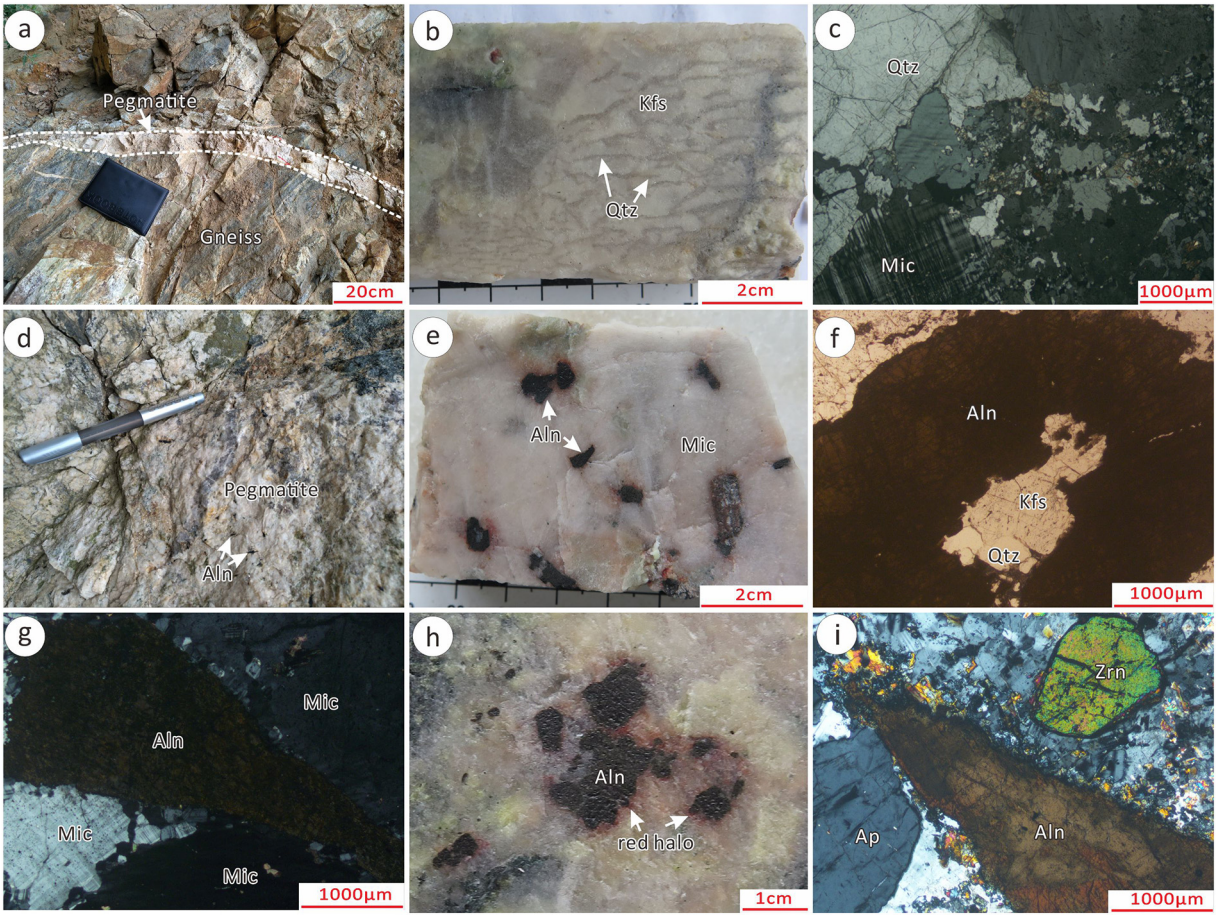

Fig. 4. Representative photographs and photomicrographs of stage I mineral assemblages at Huayangchuan deposit. (a) Pegmatite dike crosscutting gneiss. (b) Graphic texture in pegmatite. (c) Intergrowth of coarse-grained quartz and microcline. (d–e) Coarse-grained, euhedral, and black/brown disseminated callanite in pegmatite. (f–g) Coarse-grained, euhedral to subhedral, and brown callanite coexists with microcline and quartz. (h) Allanite with reddish rim. (i) Intergrowth of allanite with zircon and apatite. c, g and i: Cross-polarized light; f: Plane-polarized light. Kfs = K-feldspar, Qtz = quartz, Mic = microcline, Aln = allanite, Ap = apatite, Zrn = zircon.

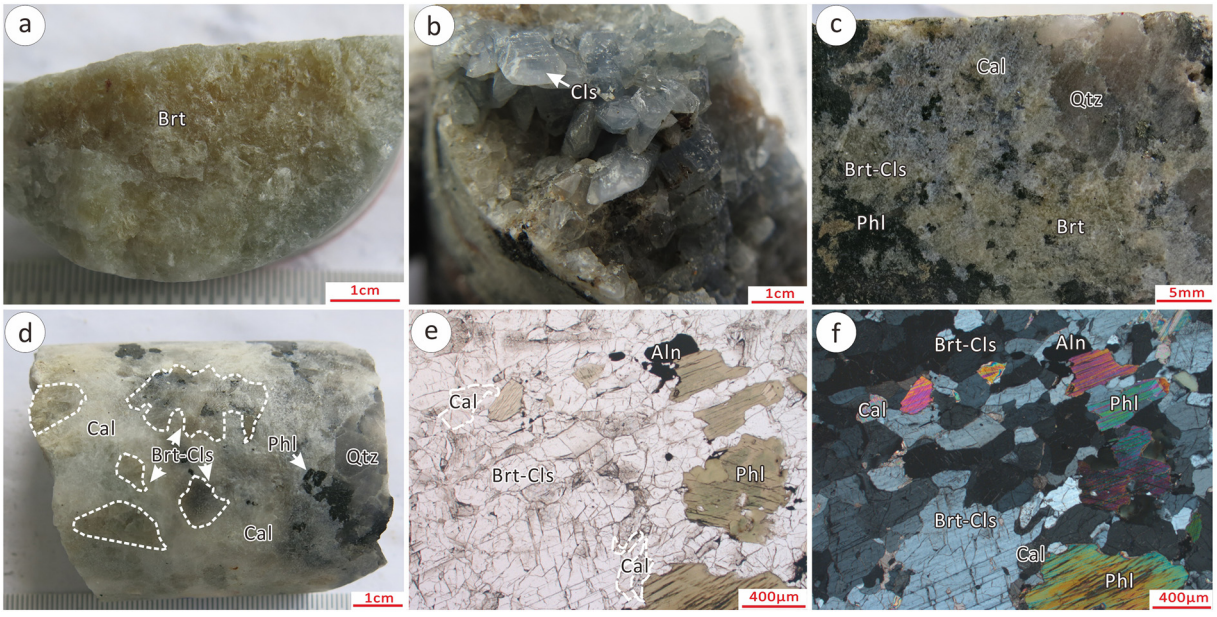

Fig. 5. Representative photographs and photomicrographs of stage II-A mineral assemblages at Huayangchuan deposit. (a) Light-yellow barite. (b) Cerulean celestite. (c) Yellowish-green barite-celestite coexist with calcite. (d) Mega-aggregate barite-celestite intergrown with calcite and phlogopite. (e–f) Barite-celestite coexist with calcite and phlogopite. e and f: Plane-polarized and cross-polarized light, respectively. Brt = barite, Cls = celestite, Cal = calcite, Aln = allanite, Phl = phlogopite, Qtz = quartz.

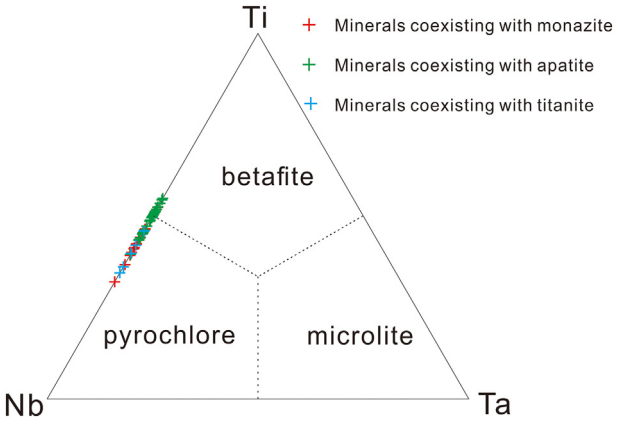

Fig. 6. Pyrochlore group classification diagram of the Huayangchuan deposit.

amphibole, biotite and allanite, is not U mineralized. Coarse-grained subhedral yellowish uranothorite usually intergrows with pyrochlore (Fig. 7i), but is absent in Stage II-C mineralization.

o (3) Stage II-C: REE-U mineralization

In this substage, REE minerals include mainly monazite and allanite, and minor chevkinite. Uranium minerals include mainly pyrochlore (UO_2: 25.18–31.71 wt%; Nb_2O_5: 30.08–42.24 wt%; TiO_2: 11.97–19.92 wt%; CaO: 6.02–17.91 wt%; FeO: 0.32–2.14 wt%; PbO: 0.27–0.71 wt%; Table 1), which plots mainly in the betafite field and minor in the pyrochlore field (Fig. 6). This substage also has minor uraninite.

The Stage II-C calcite-REE-U ore veins commonly cut the Archean gneiss (Fig. 8a–b) and the early-stage pegmatite (Fig. 8c). The REE ore minerals commonly coexist with white/light-pink calcite and form massive aggregates in the host rocks (Fig. 8d). The euhedral, fine-medium grained (50–100 μm) monazite is commonly light-yellow (in hand-specimens), and the monazite aggregates contain fine-grained euhedral pyrochlore (Fig. 8d–f). Different from the coarse-grained euhedral Stage I allanite in pegmatite (Fig. 4e), Stage II-C allanite is commonly fine-grained subhedral-anhedral, black or dark-grey (Fig. 8d–e), and usually developed in the monazite grains/aggregates (Fig. 8e–f) or filled in cleavages of coarse-grained phlogopite (Fig. 8e). Stage II-C allanite contains higher REE and lower ThO_2 contents than its Stage I counterpart (Supplementary Data). In hand-specimens, Stage II-C pyrochlore is

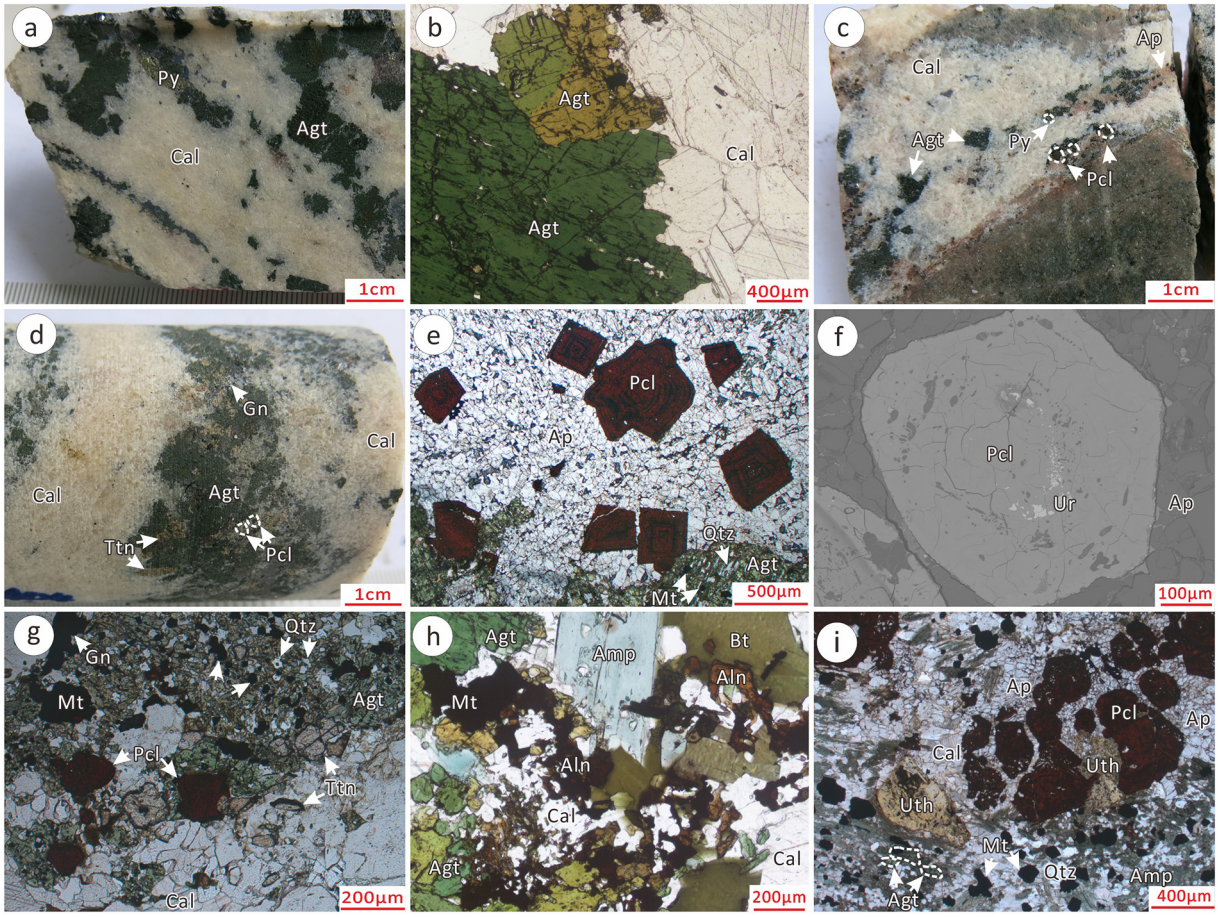

Fig. 7. Representative photographs and photomicrographs of stage II-B mineral assemblages t Huayangchuan deposit. (a–b) Coarse-grained, euhedral-subhedral, and dark green aegirine-augite coexists with calcite. (c) Pyrochlore intergrown with the assemblage of apatite, aegirine-augite and pyrochlore in carbonatite. (d) Pyrochlore coexists with titanite, aegirine-augite and galena in carbonatite. Note that some titanite crystals are present in coarse-grained euhedral envelope shape. (e) Euhedral pyrochlore with growth zoning intergrown with apatite aggregates. (f) Uraninite in the interior of pyrochlore crystal. (g) Pyrochlore and titanite intergrown with aegirine-augite, which is commonly replaced by quartz and magnetite. (h) Aegirine-augite, amphibole, biotite, and anhedral brown allanite coexist with calcite. (i) Subhedral yellow uranothorite occurs with pyrochlore, apatite, amphibole, magnetite and quartz. e, g–h: plane-polarized light, f: backscattered electron (BSE) imaging. Py = pyrite, Agt = aegirine-augite, Cal = calcite, Pcl = pyrochlore, Ap = apatite, Ttn = titanite, Gn = galena, Mt = magnetite, Qtz = quartz, Ur = uraninite, Amp = amphibole, Aln = allanite, Bt = biotite, Uth = uranothorite.

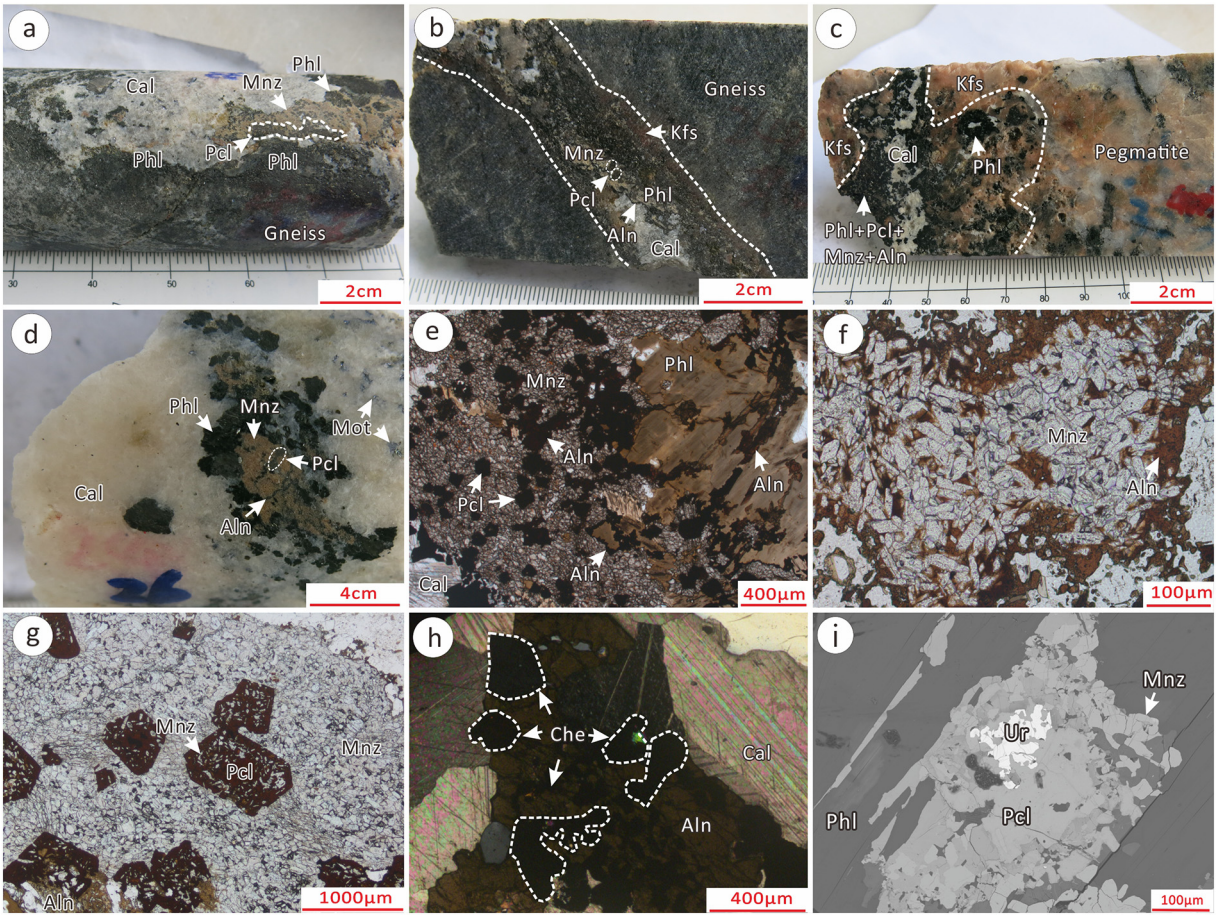

Fig. 8. Representative photographs and photomicrographs of stage II-C mineral assemblages at Huayangchuan deposit. (a–b) REE-U mineralized carbonatite occurs as veins in the gneiss, with calcite commonly coexisting with aggregates of monazite, pyrochlore, allanite and phlogopite. (c) Carbonatite vein containing calcite, phlogopite, pyrochlore, monazite and allanite cutting pegmatite, with K-feldspar at the boundary. (d) Yellow monazite aggregates coexist with calcite, pyrochlore, allanite phlogopite and molybdenite in carbonatite. (e) Fine-grained monazite coexists with pyrochlore, phlogopite and allanite. Note that pyrochlore commonly occurs as fine-grained, euhedral, and crimson crystals. Brown allanite usually fills the cleavage of coarse-grained phlogopite. (f) Colorless and high-relief monazite coexists with allanite. (g) Medium-grained pyrochlore intergrown with monazite aggregate. (h) Allanite with chevkinite coexists with calcite. (i) Intergrowth of uraninite with pyrochlore, monazite, and phlogopite. e–g: plane-polarized light; i: BSE imaging. Mnz = monazite, Cal = calcite, Aln = allanite, Phl = phlogopite, Pcl = pyrochlore, Mot = molybdenite. Che = chevkinite, Ur = uraninite, Kfs = K-feldspar.

usually red to brown, fine-medium-grained euhedral-subhedral (Fig. 8a–b), and commonly coexists with monazite (Fig. 8e and g). Chevkinite is locally common and hardly distinguishable from allanite due to their similar feature in hand-specimens and under the microscope (Fig. 8h). Uraninite is also an important U-bearing mineral in Stage II-C, and is commonly fine-grained and coexists with pyrochlore and monazite in the phlogopite (Fig. 8i).

Stage III: Skarn mineralization

Typical skarn minerals, including (prograde) garnet and pyroxene, (retrograde) amphibole and biotite, and magnetite, pyrite, galena and quartz overprinting in early carbonatite-hosted mineral assemblages, or crosscutting them as veins (Fig. 9a–b). Prograde skarn and retrograde minerals are commonly replaced by sulfides (galena and pyrite) and quartz (Fig. 9c). Stage III garnet is commonly reddish-yellow (Fig. 9a–b) and occurs as pseudomorphs replaced by galena (Fig. 9c). Stage III garnet is classified as andradite based on EPMA data (CaO: 32.05–33.16 wt%, FeO: 26.37–27.92 wt%, SiO_2: 35.54–36.17 wt%). The massive galena (Pb: 84.84–86.32 wt%, Te: 0.02–0.07 wt%, S: 13.22–13.47 wt%) occurs with minor pyrite replacing the early pegmatite and carbonatite (Fig. 9d). Trace uraninite and allanite were also formed in this stage, uraninite usually occurs on the margin of early pyrochlore or replacing it, whereas allanite is usually associated with prograde skarn minerals such as garnet and pyroxene.

Stage IV: Post-ore alteration

This stage is featured by abundant medium-coarse-grained, red, and euhedral-subhedral stilbite grains coexisting with bladed calcite and minor pyrite and galena. These minerals commonly coexist as veins cutting wallrocks or Stage I to III-altered rocks (Fig. 9e–f). Stage IV mineral assemblage (e.g., stilbite, bladed calcite and minor pyrite and galena) is extensively distributed at Huayangchuan, which represents the fading of mineralization at Huayangchuan.

6. Mineralization zoning

The minerals and mineral assemblages, based on the newly-defined paragenesis, were plotted on the main cross-section (i.e., Exploration Line 24) to unravel any alteration/mineralization zoning pattern at Huayangchuan (Figs. 2 and 10).

Minerals and mineral assemblage identification was conducted on over 500 samples from five drill-holes along Exploration Line 24. All samples were also tested for radiation anomaly, using a β-γ admeasuring apparatus FD-3010A. Mineral identification was conducted on both hand-specimens and polished thin sections under the microscope.

Delineation of the current orebody (mainly for uranium) was based on gamma-ray anomaly logging (pers. comm., #224 team of Sino Shaanxi Nuclear Industry Group) which is a quicker method than the

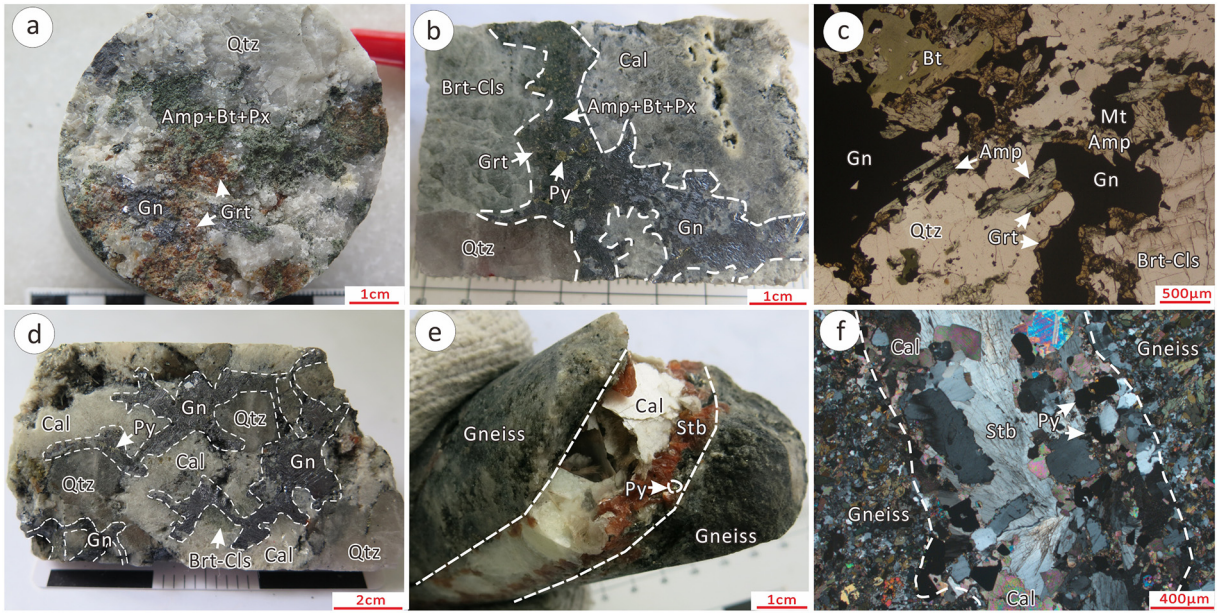

Fig. 9. Representative photographs and photomicrographs of Stage III and IV mineral assemblages at Huayangchuan deposit. (a) Typical skarn mineral assemblage includes garnet, pyroxene, amphibole, biotite, quartz, and galena. (b) Sulfide vein crosscutting carbonatite comprises calcite and barite-celestite. (c) Prograde skarn mineral assemblage of garnet, amphibole and biotite, which were replaced by magnetite, galena, and garnet showing relic texture. (d) Quartz, calcite, and barite-celestite replaced by veinlets comprising galena and minor pyrite. (e–f) The vein comprising red stilbite and bladed calcite crosscutting gneiss. c and f: plane-polarized and cross-polarized light, respectively. Amp = amphibole, Bt = biotite, Px = pyroxene, Qtz = quartz, Brt = barite, Cls = celestite, Mt = magnetite, Py = pyrite, Gn = galena, Cal = calcite, Grt = garnet, Stb = stilbite.

β-γ admeasuring apparatus FD-3010A albeit a lower accuracy. In this study, it is found that both methods produce a similar, NE-trending (NW-dipping) distribution pattern of the orebody (Fig. 10a–b). Pyrochlore, the major U-Nb ore mineral at Huayangchuan, has also a NE-dipping distribution (Fig. 10c) that coincides with the orebody defined by U anomalies. The ubiquitous Proterozoic pegmatite dikes or veins at Huayangchuan have a similar distribution pattern (Fig. 10d) to that of the carbonatites (Fig. 10e). The pyrochlore distribution pattern matches closely with that of the carbonatites (Fig. 10c and e), indicating possible genetic link between the carbonatite and U-Nb mineralization. Drill-hole ZK2405 contains the most abundant pegmatite veins and dikes in Exploration Line 24, and the pegmatite-hosted Stage I coarse-grained euhedral allanite also occurs mainly in ZK2405 (and minor in ZK2404) (Fig. 10f). Stage II-A barite-celestite mineralization has also a general NE-dipping distribution, similar to that of the carbonatite (Fig. 10g). However, distribution of Stage II-C REE-U mineralization is clearly shallower than Stage II-B alkali-rich U mineralization (Fig. 10h): the former mainly occurs in ZK2403 and ZK2402 (minor in ZK2401 and ZK2405), whereas the latter is concentrated at depth of ZK2401, 2402, 2404 and 2405 (i.e., drill-holes in the northeastern part of Line 24). The alkali-rich mineral assemblages are widely distributed (except for the ZK2403 in the SW end of Line 24), but the distribution of the ore-bearing alkali-rich mineral assemblage is clearly concentrated in the middle part compared to the ore-barren alkali-rich mineral assemblage (Fig. 10i). The skarn alteration assemblage (garnet + pyroxene + amphibole + biotite) mainly occurs in the northeastern drill-holes (ZK2401, ZK2404 and ZK2405) and shallow parts in the southwestern drill-hole (ZK2403) (Fig. 10j). Galena, the main Pb ore mineral at Huayangchuan, is much wider distributed than the prograde skarn assemblage (Fig. 10k). Stage IV stilbite is ubiquitous and occurs in all drill cores (Fig. 10l), indicating an extensive post-ore alteration at Huayangchuan.

The NE-dipping distribution of pegmatites and carbonatites coincides with the orientation of the Huayangchuan Fault (Fig. 2). Stage I allanite mineralization was likely controlled by the Proterozoic pegmatite at depth in the east. Stage II barite-celestite (Ba-Sr), pyrochlore (U and Nb), and monazite-allanite (REE) mineralization all coincide generally with the carbonatite distribution, but the substage (i.e., II-B and II-C) mineralization distribution patterns and mineral assemblages (e.g., ore-bearing/-barren alkali-rich assemblages) can be different. Skarn alteration occurs in both NW and SW of the mine, and may indicate an association with the Huashan and Laoniushan granites, respectively (Fig. 2).

7. Discussion

7.1. Uranium source at Huayangchuan

Huayangchuan is unique in its huge carbonatite-hosted uranium resource. Although alkaline melt can dissolve more U, Nb, Th and REEs than melts of other compositions (Cuney, 2009, 2012; Peiffert et al., 1996), the source of such anomalous U enrichment in the Huayangchuan carbonatite is still unclear.

The Huayangchuan carbonatite, the main U ore host, has $\delta^{13}C$ (−6.6 to −7.0‰) and $\delta^{18}O$ (7.6 to 8.4‰) (Huang et al., 2009; Xu et al., 2007) within the primary igneous carbonatite field ($\delta^{13}C$ = −3.1 to −7.7‰; $\delta^{18}O$ = 5.3 to 8.4‰; Jones et al., 2013; Taylor et al., 1967). Meanwhile, the Huayangchuan carbonatite has $^{87}Sr/^{86}Sr$ (0.704890–0.705820), $^{143}Nd/^{144}Nd$ (0.510902–0.512472), $^{206}Pb/^{204}Pb$ (17.505–18.588), $^{207}Pb/^{204}Pb$ (15.484–15.589), and $^{208}Pb/^{204}Pb$ (37.649–38.041) (Xu et al., 2007; Hui et al., 2017) resembling an EMI (Enriched Mantle I formed by lithospheric or continental crust recycling; Jones et al., 2013; Kalt et al., 1997) source region (Xu et al., 2007; Hui et al., 2017). Furthermore, recent Mg isotopes study shows that the Huayangchuan carbonatite has $\delta^{26}Mg$ (<−1.07‰; Song et al., 2016) resembling the range of marine dolomite in Mesozoic (<−1.0‰; Huang et al., 2015), and indicates significant recycled sediment inputs into the carbonatite melt (Song et al., 2016).

Although the Huayangchuan carbonatite may have been mantle derived (Huang et al., 2009; Hui et al., 2017; Xu et al., 2007), the primary upper mantle contains only very low uranium (average 0.0205 ppm; Cuney, 2009; Javoy, 1995, 1998), which could explain why most mantle-derived carbonatites do not produce significant uranium. The Huanglongpu carbonatite-hosted Mo(-Re) deposit is ca. 8 km southeast

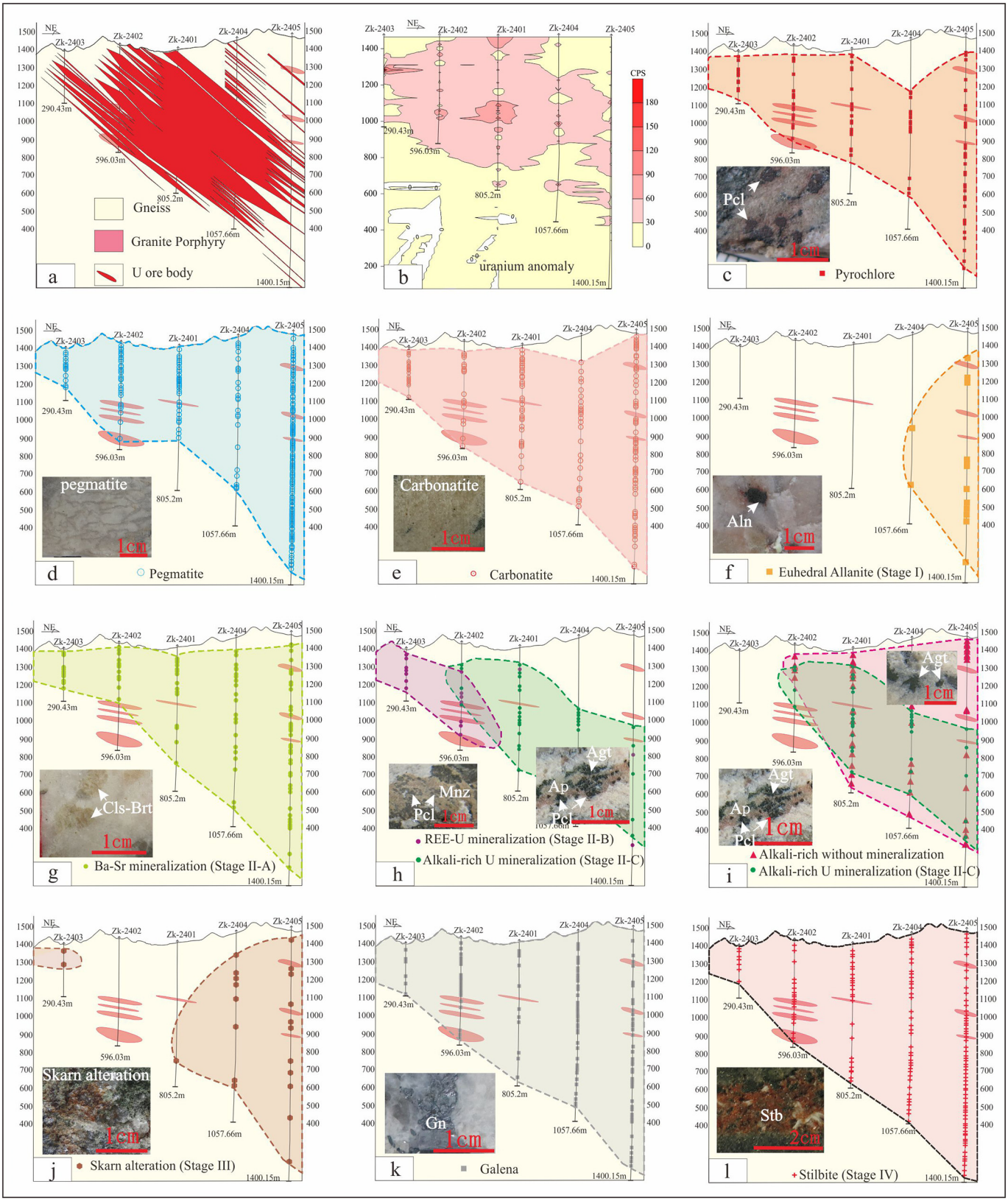

Fig. 10. Characteristics of mineralization zonation in Exploration Line 24 at Huayangchuan. (a) U ore body. (b) U anomaly. (c) Pyrochlore. (d) Pegmatite. (e) Carbonatite. (f) Coarse-grained euhedral allanite. (g) Barite-celestite. (h) REE-U mineralization and alkali-rich U mineralization. (i) Alkali-rich U mineralization and alkali-rich ore-barren. (j) Skarn alteration. (k) Galena. (l) Stilbite. Pcl = pyrochlore, Aln = allanite, Cls = celestite, Brt = barite, Mnz = monazite, Ap = apatite, Agt = aegirine-augite, Gn = galena, Bt = biotite, Stb = stilbite.

of Huayangchuan (Fig. 1) and have similar geological features and geochemistry with Huayangchuan carbonatite (Xu et al., 2007; Xu et al., 2009; Xu et al., 2011). We suggest that the high-U contents in the carbonatites at Huayangchuan and Huanglongpu may have had recycled sediment inputs into a mantle-derived magma source. Ocean sediments commonly have much higher U than normal mantle or

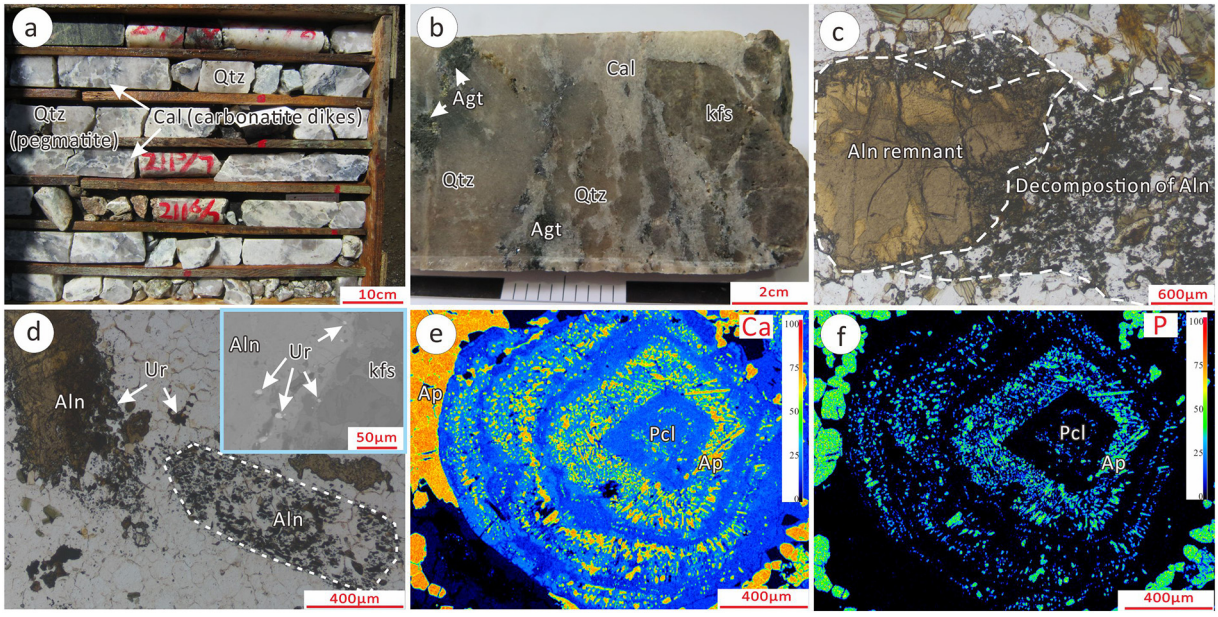

Fig. 11. Photographs and photomicrographs about uranium mineralization at Huayangchuan deposit. (a–b) Carbonatite dikes (including calcite and aegirine-augite) replacing quartz veins of pegmatite. (c) Allanite showing decomposition texture. (d) Decomposition of allanite with locally crystal shape remained, and uraninite occurred on the edge of allanite. (e–f) EPMA mapping of pyrochlore Ca and P contents, respectively. Note each circle of pyrochlore crystal contains abundant fine-grained euhedral apatite. c–d: plane-polarized light. Agt = aegirine-augite, Cal = calcite, Pcl = pyrochlore, Ap = apatite, Qtz = quartz, Aln = allanite, Ur = uraninite, Kfs = K-feldspar.

continental crust. For instance, black shale contains up to 1000 ppm U and marine phosphates contain 50–300 ppm U, compared with only <3 ppm U in average carbonate rocks (Kyser, 2014). Both Huayangchuan and Huanglongpu carbonatites contain high uranium contents. However, uranium mineralization at Huayangchuan is much more intensive than that of the Mo-dominated Huanglongpu deposit (pers. comm., #224 team of Sino Shaanxi Nuclear Industry Group). Different from Huanglongpu, the Huayangchuan carbonatite dikes/veins are always spatially associated with pegmatites (Figs. 8c and 11a), especially with megacrysts massive quartz (Fig. 11b). These Triassic carbonatite dikes commonly coexist with in spatially or crosscut the pegmatites, which are U-rich (average 39.12 ppm; Hui, 2014) and contain coarse-grained allanite grains (Fig. 4d–i). Most pegmatite-hosed allanite grains are euhedral, with some being clearly altered and have uraninite rim or pseudomorph residue (Fig. 11c–d), with locally only pseudomorphs of allanite remained (Fig. 11d). In some cases, uraninite occurs on the margin of the altered allanite (Fig. 11d). However, there is no Proterozoic pegmatite identified at Huanglongpu. This indicates that the uranium of Huayangchan deposit was mainly from both the carbonatite and the Proterozoic pegmatite.

7.2. Uranium ore formation at Huayangchuan

Uranium solubility in the silicate magmas has been extensively studied by experiments (Farges et al., 1992; Keppler and Wyllie, 1990, 1991; Peiffert et al., 1994; Peiffert et al., 1996; Zharikov et al., 1987). Oxygen fugacity and agpaicity ($\alpha = (Na + K)/Al$) are suggested to be two major factors that control uranium solubility in silicate melts. They both show positive correlations with uranium solubility, with agpaicity being much more important (Peiffert et al., 1994). Increasing the alkalinity in silicate melts would also substantially increase the uranium solubility (Farges et al., 1992; Peiffert et al., 1994; Peiffert et al., 1996). However, uranium solubility investigation in carbonatite is very rare.

Carbonatite is defined as igneous carbonate rocks with >50% carbonate minerals and high Sr, Ba, P and LREE contents (Jones et al., 2013; Le Bas, 1987; Nelson et al., 1988; Streckeisen, 1980). Compared to silicate melts, carbonate melts have lower viscosity, lower temperature of fusion, higher electrical conductivity and larger thermal diffusivity, which is a special ionic liquid (Dobson et al., 1996; Gaillard et al., 2008; Jones et al., 2013; Sifre and Gaillard, 2012; Treiman and Schedl, 1983). Carbonate ions (CO_3^{2-}) and metal cations constitute the ionic liquids of carbonate melt, the CO_3^{2-} trigonal group has no unpaired orbitals and composed of discrete unpolymerized ions unlike tetrahedra SiO_4^{4-}, and thus carbonate melts do not polymerize. In contrast, silicate melts have network structure for polymerization (Mysen, 1983, 1988; Jones et al., 2013; Treiman and Schedl, 1983). Increasing alkalinity can decrease the polymerization of silicates and enhance U solubility. Accordingly, we consider that uranium solubility in carbonatite may resemble in alkaline silicate.

At Huayangchuan, uranium is mainly hosted in pyrochlore, which is associated with carbonatites. Carbonate minerals are crystallized under extensive carbonate melt fractionation, leaving behind residual melt rich in volatiles (incl. halogens). Volatiles and halogens play vital roles in transporting uranium in the melts and fluids (Keppler and Wyllie, 1990). According to the hard-soft-acid-base principle (Pearson, 1963), uranium belongs to hard (nonpolarizable) cation, and bond preferentially with hard anions including F^-, PO_4^{3-}, CO_3^{2-} and SO_4^{2-}. According to the U solubility experiment in silicate melt and aqueous solutions with varying H_2O, HCl, HF and CO_2 contents (under 2 kbar, 750 °C and Ni-NiO buffer) (Keppler and Wyllie, 1990, 1991; Zharikov et al., 1987), uranium can combine with halogens to form U-complexes, resulting in an increase in the partition coefficient of U between fluid and melt ($Kd^{fluid/melt}$). In most magmatic uranium deposits (e.g., Bokan Mountain in Alaska), fluorine is an important halogen to transport uranium, and both U and F are enriched in highly-fractionated melts and can migrate together over a few hundred meters even kilometers (Cuney, 2012; Linnen and Cuney, 2005; Kyser and Cuney, 2009; Staatz, 1978, 1979). Besides, phosphorus can also act as an important ligand to transport uranium. For instance, the abundant apatite associated with U-rich ores of the Xiangshan U deposit (Jiangxi Province) in Eastern China indicates that the uranium likely transported in $[UO_2(HPO_4)_2]^{2-}$ complexes (Wen et al., 1999; Liu et al., 2007; Guo et al., 2018).

Pyrochlore at Huayangchuan contains some F (0.16–0.46 wt%; Supplementary Data). Euhedral pyrochlore commonly developed oscillatory zoning intergrown with apatite in the alkali-rich U ore mineral assemblage (Fig. 7e), with each growth zone containing euhedral fine-grained apatite (Fig. 11e–f). These apatite grains contain high F

(2.91–3.34 wt%), belonging to fluorapatite. Moreover, titanite intergrew with pyrochlore (Fig. 7g), which also has F (up to 0.38 wt%; Supplementary data). In the REE-U ore mineral assemblage, phlogopite intergrew with REE minerals and the pyrochlore is F-rich (up to 3.4 wt%). This suggests that F and P were likely important in transporting uranium in carbonatite melts at Huayangchuan.

Commonly, temperature and oxygen fugacity drop are two major controlling factors for uranium precipitation in many uranium deposit types, e.g., unconformity-controlled and granite-related types (Timofeev et al., 2018). However, according to the occurrence and characteristics of U-bearing pyrochlore at Huayangchuan, uranium precipitation can also be led by other factors. Pyrochlore usually precipitated where the concentration of complex anions drops sharply (Knudsen, 1989), for instance at/with (1) boundary between carbonatite and wallrocks; (2) loss of anions, such as phosphate and fluorine by apatite precipitation; (3) pressure drop that destabilizes anion complexes. Besides, pH can also control the pyrochlore precipitation. For instance, Nb-rich and Ta-rich pyrochlore is mostly soluble under neutral and acidic conditions, respectively (Knudsen, 1989). Considering the Ta-barren and Nb-rich feature of the Huayangchuan pyrochlore and its common coexistence with apatite, we deduce that the uranium was dissolved in phosphate complex under neutral conditions in carbonatite. Subsequently, the U-bearing pyrochlore may have precipitated when the environment was changed, for instance via (1) apatite (Fig. 7c and e) or monazite (Fig. 8a–g) precipitation, which consumed phosphate and destabilized the phosphate complex; and (2) major pH, temperature and pressure change along the contact between the carbonatite and wallrocks or early pegmatite (Figs. 7c and 8a–b). The few uraninite grains in the pyrochlore core (Figs. 7f and 8i) indicate that U was oversaturated in the carbonatite melt at the beginning of pyrochlore precipitation. Uraninite precipitated when uranium eventually reached saturation, followed by major pyrochlore precipitation when uranium fell back to undersaturation. At Huayangchuan, Nb is also mainly hosted in pyrochlore. According to the experimental studies by Keppler (1993), fluorine is positively correlated with the solubility of HFSEs (high field strength elements, e.g., Nb) in the melt. Nb and U share similar elemental behaviors and can be transported together in F-complexes and precipitated as pyrochlore, thus forming this special carbonatite-hosted U-Nb mineralization at Huayangchuan.

Fenitization is considered as the most important alkaline metasomatism in carbonatites (Elliott et al., 2018; Le Bas, 2008), for instance at Bayan Obo (Le Bas et al., 1992, 2007). According to their compositions, fenites are commonly divided into sodic, potassic and intermediate series (Heinrich, 1985; Le Bas, 2008; Verwoerd, 1966). Sodic fenite consists predominately of sodic pyroxene, alkali feldspar and amphibole, whereas potassic fenite is dominated by K-feldspar and mica, with minor albite, quartz and apatite (Elliott et al., 2018; Le Bas, 2008). Although lacking detailed ore-fluid physicochemical constraints, the features of mineral assemblage (Fig. 3) and fenite (Elliott et al., 2018; Le Bas, 2008) suggest that Stage II-B alkali-rich and Stage II-C REE-rich U mineralization may be associated with the sodic fenitic and potassic fenitic alteration, respectively. Based on the temperature, pressure, CO_2 content and Na_2O/K_2O in the carbonatite intrusion, Na is preferentially lost from the carbonatite melt at depth under high temperature (>600 °C), and vice versa for K enrichment in shallow-level under low temperature (<450 °C) (Elliott et al., 2018; Rubie and Gunter, 1983). This is consistent with the mineralization zoning at Huayangchuan, where alkali-rich U mineralization occurs deeper than the REE-U mineralization (Fig. 10h).

7.3. Genetic model of multistage mineralization at Huayangchuan

According to the published age and geological data at Huayangchuan-Huanglongpu district, at least three regional tectonothermal events may have occurred, i.e., the Paleoproterozoic granitic-pegmatitic magmatism, the Late Triassic granite and carbonatite magmatism, and the Early Cretaceous granitic magmatism (Table 2). We propose the following ore formation model for the Huayangchuan deposit:

1) Paleoproterozoic granitic-pegmatitic magmatism and associated REE mineralization

Table 2
Summary of representative geochronological data in the Huayangchuan district.

Deposit/pluton	Sample	Methods	Ages (Ma)	Reference
Huayangchuan	Granite	Zircon U-Pb	2420.8 ± 1.3	Hui, 2014
	Granite	Zircon U-Pb	1907.7 ± 1.4	Hui, 2014
	Granite	Zircon U-Pb	1829.5 ± 2.5	Xue et al., 2018
	Granite	Zircon U-Pb	207.1 ± 2.3	Hui, 2014
			225.5 ± 4.2	
			229.3 ± 2.7	
	Carbonatite	Phlogopite K-Ar	181	Yu, 1992
	Carbonatite	Bulk-rock K-Ar	204	Qiu et al., 1993
		Feldspar K-Ar	206	
	Carbonatite	Titanite U-Pb	209.0 ± 2.9	Zheng et al., 2020
		Molybdenite Re-Os	196.8 ± 2.4	
	Carbonatite-hosted	Biotite Ar-Ar	132.6 ± 0.7	He et al., 2016
	Pegmatite-hosted	Biotite Ar-Ar	93.7 ± 2.4	
Huanglongpu	Ilmenite	U-Th-Pb	206	Huang et al., 1984
	Molybdenite	Re-Os	220-231	Huang et al., 1994
	Molybdenite	Re-Os	221.5 ± 0.3	Stein et al., 1997
	Monazite	U-Pb	208.9 ± 4.6	Song et al., 2016
		Th-Pb	213.6 ± 4.0	
Huashan pluton	Monzonitic granite	Zircon U-Pb	133.8 ± 1.1	Guo et al., 2009
	Amphibole monzogranite	Zircon U-Pb	205 ± 2	Hu et al., 2012
	Biotite monzogranite	Zircon U-Pb	132 ± 1	
	Biotite monzonitic granite	Zircon U-Pb	142.6 ± 1.4	Zhang et al., 2015
			140.1 ± 1.2	
Laoniushan pluton	Adamellite	Zircon U-Pb	223 ± 1	Qi et al., 2012
	Quartz diorite	Zircon U-Pb	222 ± 1	
	Biotite monzogranite	Zircon U-Pb	214 ± 1	
	Biotite monzogranite	Zircon U-Pb	152 ± 1	
			146 ± 1	
	Granite porphyry	Zircon U-Pb	143.7 ± 3.0	Jiao et al., 2010
	Granite	Zircon U-Pb	144.5 ± 4.4	

In addition to the large Huashan and Laoniushan intrusive complexes in northern and southern Huayangchuan, respectively, a suite of granite (porphyry) and pegmatite intrusions or dikes were also emplaced at Huayangchuan. Xue et al. (2018) reported a zircon SIMS U-Pb age of 1829.5 ± 2.5 Ma for the Huayangchuan granite, indicating a Paleoproterozoic magmatic event. The Huayangchuan pegmatite was recently zircon U-Pb dated to be 1795 ± 50 Ma (author's unpubl. data), broadly coeval with the reported data. Zhao et al. (2004) suggested a 1.80–1.75 Ga magmatic event in the southern North China Carton (NCC) based on SHRIMP dating of the Xiong'er Gp. volcanics, which marked the beginning of the Paleoproterozoic regional rifting. Considering the large-scale Xiong'er Gp. volcanic rocks and Proterozoic intrusions distributed to the south of the Huayangchuan deposit (Fig. 1c), we speculated that the Huayangchuan granitic-pegmatitic magmatism may represent the western end-member of the 1.8 Ga magmatic event in the southern NCC. Although the highest average uranium content was detected in the Paleoproterozoic Huayangchuan granite-pegmatite (89.3 ppm; Hui, 2014), no clear U-Nb mineralization was identified to be related to these magmatic suites, whilst Proterozoic pegmatite occurred REE mineralization at Huayangchuan (Fig. 12a).

2) Late Triassic carbonatite magmatism and main U-Nb-REE-Ba-Sr mineralization

K-Ar dating of phlogopite and feldspar in the Huayangchuan carbonatites yielded Late Triassic to Early Jurassic ages (ca. 206–181 Ma, Table 2; Yu, 1992; Qiu et al., 1993). Recently, we have obtained a titanite U-Pb age (209.0 ± 2.9 Ma; Zheng et al., 2020) closely associated with main mineralization (titanite coexisting with pyrochlore in Stage II), supporting the occurrence of Indosinian carbonatite mineralization at Huayangchuan. The Huanglongpu carbonatite-hosted Mo(-Re) deposit (8 km SE of Huayangchuan) yielded ilmenite U-Pb age of ca. 206 Ma (Huang et al., 1984), molybdenite Re-Os ages of ca. 231–220 Ma (Huang et al., 1994; Stein et al., 1997), and monazite U-Th-Pb ages of ca. 214–209 Ma (Song et al., 2016), which further indicates Late Triassic regional carbonatite magmatism and associated Mo-U mineralization. Previous studies suggested that ore-bearing carbonatites (e.g., Huayangchuan, Huanglongpu, Yuantou and Huangshuian) occur along the NW-trending Luanchuan-Gushi deep-fault system in the northern Qinling Orogen margin (Huang et al., 2009). For instance, Yuantou is a carbonatite-type REE-Mo mineral occurrence in the Huanglongpu orefield (Xu et al., 2009), and Huangshuian is a large carbonatite-type Mo deposit (molybdenite Re-Os age: 209.5 ± 4.2 Ma; Huang et al., 2009). These carbonatites may have formed in a short geological period during the North China–South China collision and the Late Triassic closure of the Mianlue Ocean, which was located between the southern Qinling Orogen and northern Yangtze Block margin in the Paleozoic-Mesozoic (Chen, 2010; Song et al., 2016; Xu et al., 2014; Zhang et al., 2001).

Triassic carbonatites at Huayangchuan-Huanglongpu have distinct mantle-derived geochemical features. In particular, the U-rich recycled sediments may have contributed to the carbonatite melt during its formation in the upper mantle (Section 7.1). This initial U-rich carbonatite melt may have ascended along the deep regional faults at Huayangchuan-Huanglongpu and produced carbonatite-hosted polymetallic deposits. At Huayangchuan, the carbonatite melt may have reacted with the Paleoproterozoic high-U-REE granites and pegmatites, which further enriched the carbonatite melts with ore-forming elements. Abundant volatile components (e.g., F and P) in the carbonatite melts may have facilitated the transport of uranium and REEs in the F-/P-bearing complexes. During the multiphase injection of carbonatite melts (mostly as dikes and veins) at Huayangchuan, and controlled by temperature drop, fluid reduction and/or fenitization, U-bearing minerals (dominantly pyrochlore) may have precipitated with REE minerals and aegirine-augite assemblage, together with quartz, magnetite and sulfides (Fig. 12b).

3) Early Cretaceous granitic magmatism and Pb-(U-REE) skarn mineralization

The Late Jurassic to Early Cretaceous (Yanshanian) magmatism was an important ore-forming stage in the Qinling Orogen, and formed many giant/large porphyry Mo-(Fe-W) deposits, such as the Jinduicheng (139–129 Ma), Shangfanggou (157–134 Ma), Nannihu (157–130 Ma), Sandaozhuang (151–141 Ma) and Shijiawan (138–122 Ma) (Li et al., 2007). Intensive Yanshanian magmatism also occurred to the north and south of the Huayangchuan deposit, as represented by the Huashan granite (142–132 Ma; Guo et al., 2009; Hu et al., 2012; Zhang et al., 2015) and Laoniushan granite (152–143 Ma; Jiao et al., 2010; Qi et al., 2012), respectively.

Skarn alteration and the associated Pb (and minor U-REE) mineralization occurred mainly in the Huayangchuan carbonatites. At Huayangchuan, prograde skarn mineral assemblage is mainly distributed close to the Huashan and Laoniushan granites (Fig. 10j). The skarn-stage (Stage III) biotite yielded an ^{40}Ar-^{39}Ar age of 129 Ma (author's unpubl. data), consistent with the reported biotite Ar-Ar age of the carbonatite (132.6 ± 0.7 Ma) and the Yanshanian magmatism (He et al., 2016) at Huayangchuan. This further supports that the Yanshanian intrusions may have reacted with the Triassic carbonatites to form the Huayangchuan skarn mineralization (Fig. 12c).

8. Conclusions

(1) Four alteration/mineralization paragenetic stages were identified at Huayangchuan, i.e., Proterozoic pegmatite REE mineralization

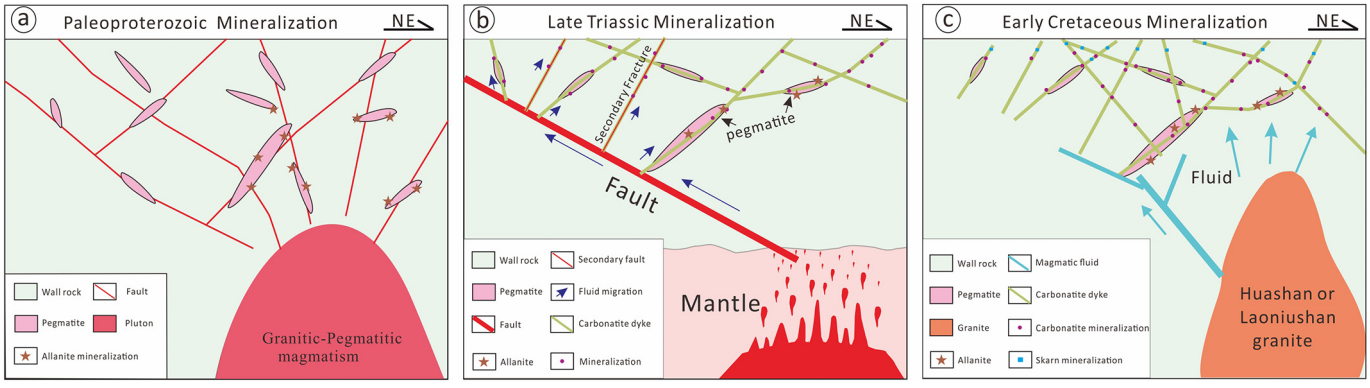

Fig. 12. Ore genesis model of the Huayangchuan deposit. (a) Paleoproterozoic granitic-pegmatitic magmatism and associated REE mineralization. (b) Late Triassic carbonatite magmatism and main U-Nb-REE-Ba-Sr mineralization. (c) Early Cretaceous granitic magmatism and skarn alteration with Pb ± U ± REE mineralization.

(I), Triassic main mineralization (II), Early Cretaceous skarn mineralization (III) and post-mineralization (IV). The main mineralization stage can be further divided into three substages, namely the sulfate mineralization (barite-celestite) (II-A), alkali-rich U mineralization (aegirine-augite + pyrochlore + uraninite + uranothorite) (II-B) and REE (allanite + monazite + chevkinite)-U (pyrochlore + uraninite) mineralization (II-C).

(2) Some ore-forming elements were introduced by recycled sediments and Proterozoic pegmatite alteration and carried in F^-, PO_4^{3-}, CO_3^{2-} and SO_4^{2-} complexes. Precipitation of U-bearing minerals may have triggered by the dilution of anionic complexes and/or fenitization. This likely formed the sodic fenite-related alkali-U mineralization at depth, and potassic fenite-related REE-U mineralization at shallow level.

(3) Pegmatite REE mineralization at Huayangchuan was broadly coeval with the intensive Proterozoic Xiong'er Gp. volcanic event in the southern margin of North China Block. The carbonatite magmatism and main U-Nb-Ba-Sr-REE mineralization may have related to the Late Triassic Mianlue Ocean closure in the South Qinling, whilst the skarn mineralization may have related to the extensive Yanshanian magmatism and porphyry-skarn Mo mineralization in the Qinling Orogen.

CRediT authorship contribution statement

Hui Zheng: Writing - original draft, Writing - review & editing, Conceptualization. **Huayong Chen:** Supervision, Project administration, Conceptualization, Funding acquisition, Writing - review & editing. **Chao Wu:** Visualization. **Hongjun Jiang:** Resources. **Cheng Gao:** Resources. **Qingqing Kang:** Resources. **Chunsi Yang:** Validation. **Dequan Wang:** Resources. **Chun-kit Lai:** Writing - review & editing.

Declaration of competing interest

The authors declare that they have no known competing financial interests or personal relationships that could have appeared to influence the work reported in this paper.

Acknowledgments

Our sincere thanks go to the staffs from Team 224 of Sino Shaanxi Nuclear Industry Group for their field support, and to Xi Chen (Southwest Petroleum University) for helping with the EPMA analysis. This study was supported by Academician Workstation of Sino Shaanxi Nuclear Industry Group (ZSH-YS180101 and ZSH-YS190101) and Chinese National Science Fund for Distinguished Young Scholars (41725009).

Appendix A. Supplementary data

Supplementary data to this article can be found online at https://doi.org/10.1016/j.gr.2020.05.016.

References

Atencio, D., Andrade, M.B., Christy, A.G., Giere, R., Kartashov, P.M., 2010. The pyrochlore supergroup of minerals: nomenclature. Can. Mineral. 48, 673–698.
Chen, Y.J., 2010. Indosinian tectonic setting, magmatism and metallogenesis in Qinling Orogen, central China. Geol. China 37, 854–865 (in Chinese with English abstract).
Chen, Y.J., Zhai, M.G., Jiang, S.Y., 2009. Significant achievement and open issues in study of orogenesis and metallogenies surrounding the North China continent. Acta Petrol. Sin. 25, 2695–2726 (in Chinese with English abstract).
Cui, H., Zhong, R., Xie, Y., Yuan, X., Liu, W., Brugger, J., Yu, C., 2019. Forming sulfate-and REE-rich fluids in the presence of quartz. Geology 48, 145–148.
Cuney, M., 2009. The extreme diversity of uranium deposits. Mineral. Deposita 44, 3–9.
Cuney, M., 2012. Uranium and Thorium. The Extreme Diversity of the Resources of the World's Energy Minerals. Springer Netherlands, pp. 91–129.
Dahlkamp, F.J., 1993. Uranium Ore Deposits. Springer, Berlin Heidelberg New York (460 pp).
Dahlkamp, F.J., 2009. Uranium Deposits of the World. Springer, Berlin Heidelberg New York (2400 pp).
Dobson, D.P., Jones, A.P., Rabe, R., Sekine, T., Kurita, K., Taniguchi, T., Kondo, T., Kato, T., Shimomura, O., Urakawa, S., 1996. In-situ measurement of viscosity and density of carbonate melts at high pressure. Earth Planet. Sci. Lett. 143, 207–215.
Elliott, H.A.L., Wall, F., Chakhmouradian, A.R., Siegfried, P.R., Dahlgren, S., Weatherly, S., Finch, A.A., Marks, M.A.W., Dowman, E., Deady, E., 2018. Fenites associated with carbonatite complexes: a review. Ore Geol. Rev. 93, 38–59.
Farges, F., Ponader, C.W., Calas, G., Brown Jr., G.E., 1992. Structural environments of incompatible elements in silicate glass/melt systems: II. UIV, UV, and UVI. Geochim. Cosmochim. Acta 56, 4205–4220.
Gaillard, F., Malki, M., Iacono-Marziano, G., Pichavant, M., Scaillet, B., 2008. Carbonatite melts and electrical conductivity in the asthenosphere. Science 322, 1363–1365.
Gao, C., Kang, Q.Q., Jiang, H.J., Zheng, H., Li, P., Zhang, X.M., Li, L., Dong, Q.Q., Ye, X.C., Hu, X.J., 2017. A unique uranium polymetallic deposit discovered in the Qinling orogenic belt: the Huayangchuan super-large U-Nb-Pb-REE deposit associated with pegmatites and carbonatites. Geochimica 46, 449–455 (in Chinese with English abstract).
Groves, D.I., Vielreicher, N.M., 2001. The Phalabowra (Palabora) carbonatite-hosted magnetite–copper sulfide deposit, South Africa: an end-member of the iron-oxide copper–gold–rare earth element deposit group? Mineral. Deposita 36, 189–194.
Guo, B., Zhu, L.M., Li, B., Fong, H.J., Wang, J.Q., 2009. Zircon U-Pb age and Hf isotope composition of the Huashan and Heyu granite plutons at the of southern margin of North China Craton: implications for geodynamic setting. Acta Petrological Sinica 25, 265–281 (in Chinese with English abstract).
Guo, J., Li, Z., Nie, J., Huang, Z., Wang, J., Lai, C.K., 2018. Genesis of Pb–Zn mineralization beneath the Xiangshan uranium orefield, South China: constraints from H–O–S–Pb isotopes and Rb–Sr dating. Resour. Geol. 68 (3), 275–286.
He, S., Li, Z.Y., Hui, X.C., Guo, J., 2016. $^{40}Ar/^{39}Ar$ geochronology of biotite in Huyangchuan uranium-polymetallic deposit in Shaanxi Province and its geological significance. Uranium Geology 32, 159–164 (in Chinese with English abstract).
Heinrich, E.W., 1985. Infinite variations on a fenite theme. Indian Mineralogy Sukheswala 151–162.
Hogarth, D.D., 1977. Classification and nomenclature of the pyrochlore group. Am. Mineral. 62, 403–410.
Hu, J., Jiang, S.Y., Zhao, H.X., Shao, Y., Zhang, Z.Z., Xiao, E., Wang, Y.F., Dai, B.Z., Li, H.Y., 2012. Geochemistry and petrogenesis of the Huashan granites and their implications for the Mesozoic tectonic settings in the Xiaoqinling gold mineralization belt, NW China. J. Asian Earth Sci. 56, 276–289.
Huang, D.H., Wang, Y.C., Nie, F.J., Jiang, X.J., 1984. Isotopic composition of sulfur, carbon and oxygen and source material of the Huanglongpu carbonatite vein-type of molybdenum(lead) deposits. Acta Geol. Sin. 58, 252–264 (in Chinese with English abstract).
Huang, D.H., Wu, C.Y., Du, A.D., He, H.L., 1994. Re-Os isotope ages of molybdenite deposits in east Qinling and their significance. Mineral Deposits 13, 221–230 (in Chinese with English abstract).
Huang, D.H., Hou, Z.Q., Yang, Z.M., Li, Z.Q., Xu, D.X., 2009. Geological and geochemical characteristics, metallogenetic mechanism and tectonic setting of carbonatite vein type Mo (Pb) deposits in the East Qinling molybdenum ore belt. Acta Geol. Sin. 83, 1968–1984 (in Chinese with English abstract).
Huang, K.J., Shen, B., Lang, X.-G., Tang, W.-B., Peng, Y., Ke, S., Kaufman, A.J., Ma, H.-R., Li, F.-B., 2015. Magnesium isotopic compositions of the Mesoproterozoic dolostones: implications for Mg isotopic systematics of marine carbonates. Geochim. Cosmochim. Acta 164, 333–351.
Hui, X.C., 2014. Geochemical Study on Uranium Polymetallic Mineralization in Huayangchuan, Shaanxi Province. (Ph.D thesis). Beijing Geological Research Institute of Nuclear Industry.
Hui, X.C., He, S., 2016. Mineralization characteristic of carbonatite veins in Huayangchuan U-polymetal deposit, Shaanxi province. Uranium Geology 32, 93–98 (in Chinese with English abstract).
Hui, X.C., Cai, Y.Q., He, S., Feng, Z.S., 2017. Petrologic and geochemical characteristics of carbonatites in Huayangchuan U-Nb-Pb deposit, Shaanxi Province. Geoscience 31, 246–257 (in Chinese with English abstract).
Javoy, M., 1995. The integral enstatite chondrite model of the Earth. Geophys. Res. Lett. 22, 2219–2222.
Javoy, M., 1998. The birth of the Earth's atmosphere: the behaviour and fate of its major elements. Chem. Geol. 147, 11–25.
Jiao, J.G., Tang, Z.L., Qian, Z.Z., Yuan, H.C., Yan, H.Q., Sun, T., Xu, G., Li, X.D., 2010. Metallogenic mechanism, magma source and zircon U-Pb age of Jinduicheng Granitic Porphyry, East Qinling. Earth Sci. 35, 1011–1022 (in Chinese with English abstract).
Jones, A.P., Genge, M., Carmody, L., 2013. Carbonate melts and carbonatites. Rev. Mineral. Geochem. 75, 289–322.
Kalt, A., Hegner, E., Satir, M., 1997. Nd, Sr, and Pb isotopic evidence for diverse lithospheric mantle sources of East African Rift carbonatites. Tectonophysics 278, 31–45.
Keppler, H., 1993. Influence of fluorine on the enrichment of high field strength trace elements in granitic rocks. Contrib. Mineral. Petrol. 114, 479–488.
Keppler, H., Wyllie, J., 1990. Role of fluids in transport and fractionation of uranium and thorium in magmatic processes. Nature 348, 531–533.
Keppler, H., Wyllie, J., 1991. Partitioning of Cu, Sn, Mo, W, U, and Th between melt and aqueous fluid in the systems haplogranite-H_2O—HCl and haplogranite-H_2O—HF. Contrib. Mineral. Petrol. 109, 139–150.
Knudsen, C., 1989. Pyrochlore Group Minerals From the Qaqarssuk Carbonatite Complex. Lanthanides, Tantalum and Niobium. Springer-Verlag, Berlin and Heidelberg, pp. 80–99.
Kyser, K., 2014. Uranium Ore Deposits // Treatise on Geochemistry. Elsevier, pp. 489–513.

Kyser, K., Cuney, M., 2009. Geochemical characteristics of uranium and analytical methodologies. In: Cuney, M., Kyser, K. (Eds.), Recent and Not-so-recent Developments in Uranium Deposits and Implications for Exploration. Mineralogical Association of Canada (MAC) and Society Geology Applied to Mineral Deposits (SGA), pp. 23–57.
Le Bas, M.J., 1987. Nephelinites and carbonatites. Geol. Soc. Lond., Spec. Publ. 30, 53–83.
Le Bas, M.J., 2008. Fenites associated with carbonatites. Can. Mineral. 46, 915–932.
Le Bas, M.J., Kellere, J., Tao, K., Wall, F., William, C.T., Zhang, P., 1992. Carbonatite dykes at bayan Obo, inner Mongolia, China. Mineral. Petrol. 46, 195–228.
Le Bas, M.J., Yang, X.M., Taylor, R.N., Spiro, B., Milton, J., Peishan, Z., 2007. New evidence from a calcite-dolomite carbonatite dyke for the magmatic origin of the massive Bayan Obo ore-bearing dolomite marble, Inner Mongolia. China. Mineral. Petrol. 90, 223–248.
Li, N., Chen, Y.J., Zhang, H., Zhang, T.P., Deng, X.H., Wang, Y., Ni, Z.Y., 2007. Molybdenum deposits in East Qinling. Earth Science Frontiers 14, 186–198 (in Chinese with English abstract).
Linnen, R.L., Cuney, M., 2005. Granite-related rare-element deposits and experimental constraints on Ta-Nb-W-Sn-Zr-Hf mineralization. In: Linnen, R.L., Samson, I.M. (Eds.), Rare-Element Geochemistry and Mineral Deposits. Geological Association of Canada. Short Course Notes 17. Geological Association of Canada, St. John's, pp. 45–67.
Liu, Z.Y., Du, L.T., Weng, Z.J., 2007. The geochemical experimental study on the relationship between uranium and phosphor in Xiangshan rich uranium mineralization. Journal of East China Institute of Technology 30, 101–106 (in Chinese with English abstract).
Mysen, B.O., 1983. The structure of silicate melts. Annu. Rev. Earth Planet. Sci. 11, 75–97.
Mysen, B.O., 1988. Structure and Properties of Silicate Melts. Elsevier.
NEA/IAEA, 2016. Uranium 2016: Resources, Production and Demand Nuclear Energy Agency and the International Atomic Energy Agency. (550 pp).
Nelson, D.R., Chivas, A.R., Chappell, B.W., McCulloch, M.T., 1988. Geochemical and isotopic systematics in carbonatites and implications for the evolution of ocean-island sources. Geochim. Cosmochim. Acta 52, 1–17.
Pearson, R.G., 1963. Hard and soft acids and base. Journal of the American Chemistry Society 85, 103–107.
Peiffert, C., Cuney, M., Nguyen-Trung, C., 1994. Uranium in granitic magmas: part 1. Experimental determination of uranium solubility and fluid-melt partition coefficients in the uranium oxide-haplogranite-H_2O-Na_2CO_3 system at 720–770°C, 2 kbar. Geochim. Cosmochim. Acta 58, 2495–2507.
Peiffert, C., Nguyen-Trung, C., Cuney, M., 1996. Uranium in granitic magmas: part 2. Experimental determination of uranium solubility and fluid-melt partition coefficients in the uranium oxide-haplogranite-H_2O-NaX (X=Cl, F) system at 770°C, 2 kbar. Geochim. Cosmochim. Acta 60, 1515–1529.
Qi, Q.J., Wang, X.X., Ke, C.H., Li, J.B., 2012. Geochronology and origin of the Laoniushan complex in the southern margin of North China Block and their implications: new evidences from zircon dating, Hf isotopes and geochemistry. Acta Petrol. Sin. 28, 279–301 (in Chinese with English abstract).
Qiu, J.X., Yu, X.H., Zeng, G.C., Li, C.N., Wang, S.J., 1993. The Alkaline Rocks of Qinling-Bashan. Geology Publishing House, Beijing (in Chinese).
Reguir, E.P., Chakhmouradian, A.R., Pisiak, L., Halden, N.M., Yang, P., Xu, C., Kynický, J., Couëslan, C.G., 2012. Trace-element composition and zoning in clinopyroxene- and amphibole-group minerals: Implications for element partitioning and evolution of carbonatites. Lithos 128, 27–45.
Rubie, D.C., Gunter, W.D., 1983. The role of speciation in alkaline igneous fluids during fenite metasomatism. Contrib. Mineral. Petrol. 82, 165–175.
Sifre, D., Gaillard, F., 2012. Electrical Conductivity Measurements on Hydrous Carbonate Melts at Mantle Pressure (EGU General Assembly Conference Abstracts).
Song, W., Xu, C., Smith, M.P., Kynicky, J., Huang, K., Wei, C., Zhou, L., Shu, Q., 2016. Origin of unusual HREE-Mo-rich carbonatites in the Qinling orogen, China. Science Reports 6, 37377.
Staatz, M.H., 1978. I and L uranium and thorium vein system, Bokan Mountain, southeastern Alaska. Econ. Geol. 73, 512–523.
Staatz, M.H., 1979. Geology and mineral resources of the Lemhi Pass thorium district, Idaho and Montana. USGS Professional Paper 1049-A (90 p).
Stein, H.J., Markey, R.J., Morgan, J.W., Du, A., Sun, Y., 1997. Highly precise and accurate Re-Os ages for molybdenite from the East Qinling molybdenum belt, Shaanxi Province, China. Econ. Geol. 92, 827–835.
Streckeisen, A., 1980. Classification and nomenclature of volcanic rocks, lamprophyres, carbonatites and melilitic rocks IUGS Subcommission on the systematics of igneous rocks. Geol. Rundsch. 69, 194–207.
Taylor Jr., H.P., Frechen, J., Degens, E.T., 1967. Oxygen and carbon isotope studies of carbonatites from the Laacher See District, West Germany and the Alnö District, Sweden. Geochim. Cosmochim. Acta 31, 407–430.
Timofeev, A., Migdisov, A.A., Williams-Jones, A.E., Roback, R., Nelson, A.T., Xu, H., 2018. Uranium transport in acidic brines under reducing conditions. Nat. Commun. 9, 1–7.
Treiman, A.H., Schedl, A., 1983. Properties of carbonatite magma and processes in carbonatite magma chambers. The Journal of Geology 91, 437–447.
Verwoerd, W.J., 1966. South African carbonatites and their probable mode of origin. Annual University Stellenbosch 41, 121–233.
Wang, L.J., Xu, C., Wu, M., Song, W.L., 2011. A study of fluid inclusion from Huayangchuan Carbonatite. Acta Mineralogica Sin. 31, 372–379 (in Chinese with English abstract).
Wen, Z.J., Du, L.T., Liu, Z.Y., 1999. Ore-forming model of the extremely-rich ores in Xiangshan Uranium Orefield, Jiangxi. Geological Review 45, 763–767 (in Chinese with English abstract).
Woolley, A.R., Kempe, D.R.C., 1989. Carbonatites: nomenclature, average chemical composition. In: Bell, K. (Ed.), Carbonatites: Genesis and Evolution. Unwin Hyman, London.
Woolley, A.R., Kjarsgaard, B.A., 2008. Paragenetic types of carbonatite as indicated by the diversity and relative abundances of associated silicate rocks: evidence from a global database. Can. Mineral. 46, 741–752.
Xie, Y.L., Hou, Z.Q., Yin, S.P., Dominy, S.C., Xu, J.H., Tian, S.H., Xu, W.Y., 2009. Continuous carbonatitic melt-fluid evolution of a REE mineralization system: Evidence from inclusions in the Maoniuping REE Deposit, Western Sichuan, China. Ore Geol. Rev. 36, 90–105.
Xu, C., Campbell, I.H., Allen, C.M., Huang, Z., Qi, L., Zhang, H., Zhang, G., 2007. Flat rare earth element patterns as an indicator of cumulate processes in the Lesser Qinling carbonatites, China. Lithos 95, 267–278.
Xu, C., Song, W.L., Qi, L., Wang, L.J., 2009. Geochemical characteristic and tectonic setting of ore-bearing carbonatite in Huanglongpu Mo ore field. Acta Petrol. Sin. 25, 422–430 (in Chinese with English abstract).
Xu, C., Taylor, R.N., Kynicky, J., Chakhmouradian, A.R., Song, W.L., Wang, L.J., 2011. The origin of enriched mantle beneath North China block: evidence from young carbonatites. Lithos 127, 1–9.
Xu, C., Chakhmouradian, A.R., Taylor, R.N., Kynicky, J., Li, W., Song, W., Fletcher, I.R., 2014. Origin of carbonatites in the South Qinling orogen: implications for crustal recycling and timing of collision between the South and North China Blocks. Geochim. Cosmochim. Acta 143, 189–206.
Xue, S., Xu, Y., Ling, M.X., Kang, Q.Q., Jiang, X.Y., Sun, S.J., Wu, K., Zhang, Z.K., Luo, Z.B., Liu, Y.L., 2018. Geochemical constraints on genesis of Paleoproterozoic A-type granite in the south margin of North China Craton. Lithos 304, 489–500.
Yu, X.H., 1992. Geological, mineralogical characteristics and origin of the carbonatites from Huayangchuan, Shaanxi Province. Earth Sci. 17, 151–158 (in Chinese with English abstract).
Zhang, G.W., Zhang, B.R., Yuan, X.C., Xiao, Q.H., 2001. Qinling Orogenic Belt and Continental Dynamics. Science Press, Beijing, pp. 1–855 (in Chinese with English abstract).
Zhang, X.L., Ye, H.S., Li, Z.Y., Cao, J., Wang, X.Y., 2015. Zircon U-Pb ages, Hf isotopic composition and geochemistry of Dafuyu granitoid pluton from Huashan complex batholith in Xiaoqinling. Mineral Deposits 34, 235–260 (in Chinese with English abstract).
Zhao, T.P., Zhai, M.G., Xia, B., Li, H.M., Zhang, Y.X., 2004. Zircon U-Pb SHRIMP dating for the volcanic rocks of the Xiong'er Group: constraints on the initial formation age of the cover of the North China Craton. Chinese Science Bulletin 49, 2495–2502 (in Chinese with English abstract).
Zharikov, V., Ivanov, I., Omel'yanenko, B., Red'Kin, A., Yudintsev, S., 1987. Experimental study of the solubility of uraninite in granitic melts and fluid solutions at high pressures and temperatures. Int. Geol. Rev. 29, 997–1004.
Zheng, H., Chen, H.Y., Li, D.F., Wu, C., Chen, X., Lai, C.-k., 2020. Timing of carbonatite-hosted U-polymetallic mineralization in the supergiant Huayangchuan deposit, Qinling Orogen: constraints from titanite U–Pb and molybdenite Re–Os dating. Geoscience Frontiers https://doi.org/10.1016/j.gsf.2020.03.001 (in press).